HHS Public Access

Author manuscript

J Phys Chem A. Author manuscript; available in PMC 2015 July 31.

Published in final edited form as:

J Phys Chem A. 2015 June 4; 119(22): 5865–5882. doi:10.1021/acs.jpca.5b03159.

Numerical Study on the Partitioning of the Molecular Polarizability into Fluctuating Charge and Induced Atomic Dipole Contributions

Ye Mei[*,†,‡,¶], **Andrew C. Simmonett**[¶], **Frank C. Pickard IV**[¶], **Robert A. DiStasio Jr.**[§], **Bernard R. Brooks**[¶], and **Yihan Shao**[*,‖]

[†]State Key Laboratory of Precision Spectroscopy, Department of Physics and Institute of Theoretical and Computational Science, East China Normal University, Shanghai 200062, China

[‡]NYU-ECNU Center for Computational Chemistry at NYU Shanghai, Shanghai 200062, China

[¶]Laboratory of Computational Biology, National Institutes of Health, National Heart, Lung and Blood Institute, 5635 Fishers Lane, T-900 Suite, Rockville, MD 20852, USA

[§]Department of Chemistry, Princeton University, Princeton, NJ 08544, USA

[‖]Q-Chem Inc., 6601 Owens Drive, Suite 105, Pleasanton, CA 94588, USA.

Abstract

In order to carry out a detailed analysis of the molecular static polarizability, which is the response of the molecule to a uniform external electric field, the molecular polarizability was computed using the finite-difference method for 21 small molecules, using density functional theory. Within nine charge population schemes (Löwdin, Mulliken, Becke, Hirshfeld, CM5, Hirshfeld-I, NPA, CHELPG, MK-ESP) in common use, the charge fluctuation contribution is found to dominate the molecular polarizability, with its ratio ranging from 59.9% with the Hirshfeld or CM5 scheme to 96.2% with the Mulliken scheme. The Hirshfeld-I scheme is also used to compute the other contribution to the molecular polarizability coming from the induced atomic dipoles, and the atomic polarizabilities in 8 small molecules and water pentamer are found to be highly anisotropic for most atoms. Overall, the results suggest that (a) more emphasis probably should be placed on the charge fluctuation terms in future polarizable force field development; (b) an anisotropic polarizability might be more suitable than an isotropic one in polarizable force fields based entirely or partially on the induced atomic dipoles.

Keywords

charge decomposition; polarizability; charge transfer; induced dipole; transferability

[*]To whom correspondence should be addressed ymei@phy.ecnu.edu.cn; yihan@q-chem.com.

Supporting Information Available

Coordinates of the molecules studied in this work, the full list of the correlations among the charge schemes and the atomic polarizabilities with the Hirshfeld-I scheme are available in the Supporting Information. This material is available free of charge via the Internet at http://pubs.acs.org

Introduction

Molecular dynamics (MD) simulations are now routinely utilized in the study of proteins and other biological molecules,[1] with the accuracy controlled by the underlying energy functions and sampling algorithms. Contemporary nonpolarizable force fields, *i.e.*, in which fixed partial charges are used for all of the atoms in the system, are the predominant methods of choice for energy functions in classical MD simulations. In addition, these methods are also widely used in hybrid quantum mechanics/molecular mechanics (QM/MM) calculations to provide electrostatic embedding potentials for the quantum mechanical (QM) atoms. Despite their popularity and success in numerous applications, nonpolarizable force fields lack an explicit description of electron response to the specific chemical environment. Thus, they have limited ability in describing the kinetics and dielectric properties of polar solvents,[2,3] charge transfer between diverse dielectric media, and the interactions between ions and π-orbitals, where this polarization effect can be rather significant.[4] This limitation also impacts QM/MM calculations in cases where mutual polarization between the QM and MM regions are required.[5–7]

To overcome this limitation, several methodologies have been proposed to explicitly account for such polarization effects in classical force fields,[8–12] and include the fluctuating charge model,[13–18] the induced multipole model,[19–27] and Drude oscillator schemes.[28–34] In addition, a hybrid scheme that combines the fluctuating charge and induced dipole models has also been developed.[35,36] Some of these polarizable force fields have been implemented in various MD simulation packages, such as AMBER,[37] CHARMM,[38] NAMD,[39] and Gromacs.[40]

In the fluctuating charge model, a molecule responds to an external electrostatic environment through charge flow between its constituent atoms. This charge redistribution restores electronegativity equality and lowers the total potential energy of the molecule. Conceptually speaking, the fluctuating charge model is simple, but unless extra “off-atom” sites are employed, this model cannot accurately describe the anisotropic response of the electron density around each atomic nucleus to an external perturbation. A notable and important example of this shortcoming is the out-of-plane distortion of the electron density associated with an aromatic ring involved in an ion-π interaction.

In the induced multipole model, a series of extra multipoles are placed on each atom that vary in response to the local electrostatic field, the extent to which is governed by pre-assigned atomic polarizabilities.[24] For example, the AMOEBA force field utilizes atomic polarizabilities that were originally proposed by Thole[41] and have been reoptimized using high-level quantum chemical calculations.[42] In the AMBER force field, the atomic polarizabilities are mainly derived from numerical fitting to the experimental molecular polarizabilities of 420 molecules obtained from the molecular refraction measurements.[24]

In the Drude oscillator model (also known as the shell model[43,44] or charge-on-a-spring model[45]), a fictitious charged particle is attached to each polarizable (parent) atom through a spring, and, together with the parent atom, forms an instantaneous local dipole which describes the local polarization. In the CHARMM implementation of the Drude oscillator

model, the atomic polarizabilities are fit to high-level quantum chemical calculations in the gas phase, but are scaled for use in condensed-phase simulations.[46] In the early (massless) implementations,[28] the position of the Drude particles (and thus the orientation and magnitude of the local dipoles) were solved for self-consistently at each confguration along a MD trajectory. More recently, the Drude particles acquired a small (fictitious) mass and thus became pseudoatoms,[32] which allows their associated positions and velocities to be updated along with other normal atoms. However, shorter MD time steps are now required to accurately integrate the corresponding equations of motion because of the relatively fast motion of the lighter Drude particles. Nonetheless, implementation of the Drude oscillator model into existing MD packages is straightforward, in which the fictitious particles are treated in essentially the same manner as standard atoms. Recently, the Drude model has also been utilized in QM/MM simulations to improve the description of the interface between the QM and MM regions.[5,47,48]

To further improve upon the accuracy and applicability of polarizable force fields, it is desirable to gain a clearer picture of the electrostatics and polarization interactions present in macromolecular systems. However, such a task can be challenging for the following reasons:

1. The electrostatics/polarization interactions are strongly coupled to bonded interactions. In this regard, bond stretching, angle bending, and/or torsional motion alter the electronic structure of a molecule, and thus its atomic multipoles; however, the related changes in the electrostatic energy are already folded into the bonded terms. As such, the 1-2 and 1-3 nonbonded (electrostatics and van der Waals) interactions are completely omitted while the 1-4 nonbonded interactions may be scaled down in most widely used force fields.

2. The distinction between permanent electrostatics and instantaneous polarization is equally, if not more, vague in this context, because such a distinction heavily depends on the reference structure(s) from which the parameters describing the permanent electrostatics are derived. To the extent that the atomic partial charges are often fitted from condensed-phase calculations and/or averaged over multiple conformations,[49–58] most nonpolarizable force fields in widespread use today actually utilize “prepolarized” parameters for the permanent electrostatics.[59] In some MD simulations, one uses a “polarized” force field with atomic partial charges that are periodically refitted or updated on the fly.[54,60]

3. As Söderhjelm *et al.*[61] discussed, the external electrostatic potential and field at the molecular fragment under consideration can also be highly non-uniform. This in turn will affect the accuracy of some polarizable force fields, as current implementations of the fluctuating charge model only utilize the local electrostatic potential at the nuclear positions while the induced multipole model only uses the local electrostatic field at these positions in space.

4. In a molecule, the atomic partial charges, dipole moments, higher-order multipole moments, and polarizabilities, all of which are central to current nonpolarizable and polarizable force fields, are not physical observables. While these quantities can be

parameterized through extensive simulations to reproduce condensed-phase experimental data,[62] the dominant approach is still to fit them to *ab initio* QM calculations. There, in addition to the obvious dependence on the QM method and the chosen basis set, the parameterization of these "atomic" quantities also varies with the decomposition/localization scheme employed for dividing molecular properties (densities, polarizabilities, etc.) into atomic contributions.[63–65]

In view of these challenges, we seek to gain a deeper understanding of polarization effects in this work by analyzing the static polarizabilities of 21 representative molecular systems using a finite-difference approach. In this work, all of the molecules were studied at their equilibrium geometries, so the aforementioned bonded terms will not affect the electronic structure at all. In this regard, it is convenient to use the electronic structure of a given molecule in the absence of an external electrostatic field as the reference, which allows for a clear separation between the permanent electrostatics and the instantaneous polarization. In a finite-difference calculation, a uniform external electrostatic field is applied in six different directions (±x, ±y, ±z) — this partially addresses the third issue above (non-uniform external electrostatic potential and field), but admittedly the *effective* electrostatic potential and field at and around the atoms can still be somewhat non-uniform. (In a related work, the polarization effects on the molecular electronic structure within the external non-uniform electrostatic potential due to solvent molecules or a protein were studied numerically.[66])

This approach will allow us to focus on the last issue above, *i.e.*, the partitioning of molecular polarizabilities into atomic polarizabilities, with the goal of improving the parameterization of advanced classical force fields. More specifically, nine charge population schemes (Mulliken, Löwdin, natural population analysis (NPA), electrostatic potential based charge (ESP), CHELPG, Hirshfeld, iterative Hirshfeld (abbreviated as Hirshfeld-I hereafter), charge model 5 (CM5), and Becke) were used to compute the fluctuating charge contributions to the static molecular polarizabilities. With four schemes (Mulliken, Hirshfeld, Hirshfeld-I, and Becke), for which atom-in-molecule densities are clearly defined, the induced atomic dipoles and thus the atomic polarizabilities were also computed, and the transferability of these approaches between different molecules was examined. Furthermore, the dependence on the specific density functional approximations and the underlying one-particle basis sets was also analyzed herein.

Theory and Computational Details

Charge Definitions

Despite their widespread use in molecular modeling, atomic charges are not physical observables and thus do not have a unique definition that can be rigorously derived from quantum mechanics. As a result, numerous models have been developed over the past several decades for computing atomic charges. According to Truhlar and coworkers,[67,68] these models fall into the following four general categories:

Class I charge models—These models do not have a solid quantum mechanical foundation. Instead, they are derived from classical mechanical models such as classical

electronegativity equalization[14,69,70] or from experimental measurements, for instance, of the electron density from X-ray diffraction.[71]

Class II charge models—These models are based on charge partition schemes, in which the electron density obtained from a quantum mechanical calculation is allotted to the atoms in the molecule. Several partition schemes have been proposed, and include Mulliken population analysis,[72,73] Löwdin population analysis,[74,75] atom-in-molecule (AIM) population analysis,[76] natural population analysis (NPA),[77,78] Hirshfeld population analysis,[79] Hirshfeld-I population analysis,[80] and Becke population analysis.[81]

The Mulliken population analysis method was proposed by Mulliken in 1955, and is based on the linear combination of atomic orbitals-molecular orbital (LCAO-MO) method.[72,73] In this method, the Mulliken charge is calculated as

$$Q_A^{\mathrm{Mulliken}} = Z_A - \sum_{\mu \in A} (\mathbf{PS})_{\mu\mu}, \quad (1)$$

where Z_A is the nuclear charge, **P** is the density matrix which depends on the occupied molecular orbital coefficients ($C_{\mu i}$), *i.e.*,

$$P_{\mu\nu} = \sum_{i \in occ} C_{\mu i} C_{\nu i} \quad (2)$$

and **S** is the overlap matrix between atomic orbitals (μ, ν), and *i* refer to occupied molecular orbitals.

The Löwdin charge is defined as

$$Q_A^{L\ddot{o}wdin} = Z_A - \sum_{\mu \in A} \left(\mathbf{S^{1/2}PS^{1/2}}\right)_{\mu\mu}, \quad (3)$$

which is based on a symmetric matrix, $\mathbf{S^{1/2}PS^{1/2}}$ (as opposed to the nonsymmetric **PS** for the Mulliken charge in Eq. 1).

NPA charge, the natural charge for an atom, is the sum of the natural populations from the natural bond orbital (NBO) analysis.[77] NBO analysis localizes and classifies the orbitals into bonding, antibonding, nonbonding, and Rydberg types. Only the bonding orbitals are shared between atoms and are partitioned in a similar way as the Mulliken population analysis above.

In the Hirshfeld partition scheme,[79] the molecular electron density $\rho_{mol}(\vec{\mathbf{r}})$ is partitioned into a sum of atomic densities, $\rho_A(\vec{\mathbf{r}})$, *via* the following weight functions, $\omega_A(\vec{\mathbf{r}})$:

$$\begin{aligned} \rho_A(\vec{\mathbf{r}}) &= \omega_A(\vec{\mathbf{r}})\,\rho_{mol}(\vec{\mathbf{r}}) \\ &= \frac{\rho_A^0(\vec{\mathbf{r}})}{\sum_B \rho_B^0(\vec{\mathbf{r}})}\rho_{mol}(\vec{\mathbf{r}}), \end{aligned} \quad (4)$$

in which $\rho_X^0(\vec{\mathbf{r}})$ is the electron density of an isolated atom *X* in vacuum. The Hirshfeld atomic charges are thus defined as

$$Q_A^{\text{Hirshfeld}} = Z_A - \int d\vec{\mathbf{r}}\, \rho_A(\vec{\mathbf{r}}), \quad (5)$$

and tend to be quite small.[80] Hence, this scheme significantly underestimates the molecular dipole moment if only atomic charges are used (in other words, the atomic dipoles that are defined later as the second term in Eq. 13 are significant). Besides, the selection of the promolecular density, $\sum_B \rho_B^0(\vec{\mathbf{r}})$, is somewhat arbitrary and it has been shown that the computed Hirshfeld charges can depend substantially on the definition of the promolecular density.[82]

In order to increase the molecular dipole moments as predicted from atomic charges (*i.e.*, to enhance the charge separation), several variations/extensions of the Hirshfeld population analysis have been proposed, including Hirshfeld-I,[80] Fractional Occupation Hirshfeld-I method (FOHI),[83,84] Iterative Stockholder Analysis (ISA)[85,86] and its Gaussian variant[87] as well as density-derived electrostatic and chemical (DDEC) charge,[88–90] which is a combination of Hirshfeld-I and ISA. The main strategy in all of these methods is to generate atomic densities with a fractional number of electrons for each atom in a self-consistent manner. For instance, in the Hirshfeld-I scheme, for an atom with $N_A + \Delta_A$ electrons and $\Delta_A \in [0, 1]$ (and thus a net charge of $Z_A - N_A - \Delta_A$), its atomic density is defined as an interpolation between the atomic charge densities with N_A (floor) and $N_A + 1$ (ceiling) number of electrons,

$$\rho_A = \rho_A^{(N_A)} + \Delta_A \left[\rho_A^{(N_A+1)} - \rho_A^{(N_A)}\right]. \quad (6)$$

These interpolated atomic densities are then utilized to compute atomic charges in the next iteration, and this procedure continues until convergence is reached. However, a recent study showed that the Hirshfeld-I scheme sometimes overshoots the deficiency of the Hirshfeld population analysis and leads to overestimated molecular dipole moments.[91]

Originally, Becke weights[81] were proposed for dividing integrals over the entire molecular volume into atomic sums, making the integration more convenient to compute. The Becke weights, $\omega_A(\vec{\mathbf{r}})$, are constructed from cell functions, P_A, which are simple polynomials in the distance between nuclei (*A*) and grid points (**r**),

$$\omega_A(\vec{\mathbf{r}}) = \frac{P_A(\vec{\mathbf{r}})}{\sum_B P_B(\vec{\mathbf{r}})}, \quad (7)$$

and satisfy the normalization condition, $\sum_A \omega_A = 1$. Then the Becke charges can be calculated as

$$Q_A^{\text{Becke}} = Z_A - \int d\vec{\mathbf{r}}\, \omega_A(\vec{\mathbf{r}})\, \rho_{mol}(\vec{\mathbf{r}}). \quad (8)$$

Becke charges are sometimes used in constrained density functional theory (CDFT) calculations[92] for the study of charge-transfer processes. In the work, we adopt the atom size adjustment[81] and the corresponding Bragg radii are 0.25 Å for H, 0.70 Å for C, 0.65 Å for N, and 0.60 Å for O atoms.

Class III charge models—Within these models, atomic charges are fitted to certain physical quantities obtained from quantum mechanical calculations, especially the electrostatic potential (ESP).[93–98] However, ESP-based charges, such as Merz-Kollman (MK-ESP) charges[96] and CHELPG charges,[98] are not strictly rotationally invariant and can suffer from numerical instabilities, which leads to difficulties in determining partial charges for buried atoms.[99,100] Accordingly, several amendments were proposed to mitigate these numerical difficulties by implementing regularization techniques,[101] appending the electronegativity equalization to the ESP fit,[102] adding more grid points and using a smooth cutoff method,[103] or by splitting atomic charges into a mean-field charge and a small perturbation.[104]

We note that another numerical issue with ESP charges comes from the appearance (or disappearance) of some grid points, even with a relatively small change in the molecular geometry/conformation. This can cause the ESP charges to have a non-smooth dependence on the molecular geometry, thereby causing difficulties during the computation of analytical derivatives of these charges with respect to the nuclear coordinates,[105] which might be required if one updates the ESP charges on the fly (like the CHELPG charges used to represent the QM electronic density in a QM/MM Ewald calculation). However, this latter issue has recently been addressed.[106,107]

Class IV charge models—With these models, atomic charges are parameterized to reproduce some observables from either experiments or high-level QM calculations.[67,68,108–110] For example, the Charge Model 5 (CM5)[68] builds upon the Hirshfeld charges *via*

$$Q_A^{CM5} = Q_A^{\text{Hirshfeld}} + \sum_{k' \neq k} T_{kk'} B_{kk'}, \quad (9)$$

where the Pauling bond order, $B_{kk'}$, is a function that approximately describes the electron density overlap between two atoms and is defined as

$$B_{kk'} = exp\left[-\alpha\left(r_{kk'} - R_{Z_k} - R_{Z_{k'}}\right)\right]. \quad (10)$$

The α parameter in Eq. 10 and the $T_{kk'}$ parameters were optimized by Marenich *et al.*.[68] It is worth noting here that the second term on the right hand side of Eq. 9 is independent of the molecular electronic structure. Therefore, CM5 and Hirshfeld charges have the same basis-set and functional dependence, and the molecular responses to the external perturbation also remains the same for these two schemes. Scaled CM5 charges have recently been used in condensed-phase modeling for computing hydration free energies.[111]

Decomposition of the Molecular Dipole Moment and Static Polarizability

With four charge models (Mulliken, Hirshfeld, Hirshfeld-I, and Becke) in use in this numerical study, the electron density of a molecule, $\rho(\vec{\mathbf{r}})$, can be decomposed into atomic densities, $\rho_A(\vec{\mathbf{r}})$, at every point in real space,

$$\rho(\vec{\mathbf{r}}) = \sum_A \rho_A(\vec{\mathbf{r}}), \quad (11)$$

and then the partial atomic charges can be computed according to Eq. 5. The electronic portion of the molecular dipole moment is

$$\vec{\boldsymbol{\mu}} = \int d\vec{\mathbf{r}}\ \vec{\mathbf{r}}\,\rho(\vec{\mathbf{r}}) = \sum_A \int d\vec{\mathbf{r}}\ \vec{\mathbf{r}}\,\rho_A(\vec{\mathbf{r}}). \quad (12)$$

Therefore, the molecular dipole moment (including both electronic and nuclear contributions) can be written as follows:

$$\begin{aligned} \vec{\boldsymbol{\mu}} &= \sum_A Q_A \vec{\mathbf{R}}_A + \sum_A \int d\vec{\mathbf{r}} \left(\vec{\mathbf{r}} - \vec{\mathbf{R}}_A\right) \rho_A(\vec{\mathbf{r}}) \\ &= \sum_A Q_A \vec{\mathbf{R}}_A + \sum_A \vec{\boldsymbol{\mu}}_A, \end{aligned} \quad (13)$$

with the first term on the right hand side corresponding to the dipole formed by atomic partial charges and the second term corresponding to local atomic dipoles.

In the computation of the static molecular polarizability tensor, which is the response of the molecular dipole moment with respect to the applied external electrostatic field,

$$\begin{aligned} \alpha_{ij} &= \left(\frac{\partial \mu_i}{\partial E_j}\right)_{E=0} \\ &= \lim_{E_j \to 0} \frac{\mu_i(E_j) - \mu_i(-E_j)}{2E_j}, \end{aligned} \quad (14)$$

where $i, j \in x, y, z$, while μ_i refers to the x, or y, or z component of the molecular dipole moment, E_j is the strength of the electrostatic field along direction j. Just like the molecular dipole moment in Eq. 13, the dipole moment difference, given in the numerator in Eq. 14, also has two contributions:

$$\begin{aligned} \Delta\vec{\boldsymbol{\mu}} &= \sum_A \Delta Q_A \vec{\mathbf{R}}_A + \sum_A \int d\vec{\mathbf{r}} \left(\vec{\mathbf{r}} - \vec{\mathbf{R}}_A\right) \Delta\rho_A(\vec{\mathbf{r}}) \\ &= \sum_A \Delta Q_A \vec{\mathbf{R}}_A + \sum_A \Delta\vec{\boldsymbol{\mu}}_A, \end{aligned} \quad (15)$$

where the first term corresponds to the charge fluctuation (migration) in the molecule, and the second term corresponds to the change in the local atomic dipoles. Accordingly, the static polarizability tensor in Eq. 14 also has the fluctuating charge (FC) and induced atomic dipole (IAD) contributions, *i.e.*,

$$\alpha_{ij} = \alpha_{ij}^{FC} + \alpha_{ij}^{IAD}, \quad (16)$$

wherein

$$\alpha_{ij}^{FC} = \lim_{E_j \to 0} \sum_A = \frac{[Q_A(E_j) - Q_A(-E_j)] R_{A,i}}{2E_j}, \quad (17)$$

$$\alpha_{ij}^{IAD} = \lim_{E_j \to 0} \sum_A \frac{\mu_{A,i}(E_j) - \mu_{A,i}(-E_j)}{2E_j}. \quad (18)$$

where $R_{A,i}$ in Eq. 17 refer to the *i*-th (x, or y, or z) coordinate of atom A.

To compute the static polarizabilities in Eq. 14, we used a finite difference approach, wherein an external electrostatic field of 10^{-3} a.u. was applied in the $\pm x$, $\pm y$, $\pm z$ directions. In Eq. 14, one cancels out all even-order (0, 2, 4, …) responses in the molecular dipole moments, leaving only the odd-order (1, 3, 5, …) responses. Increasing the field strength by 1 order of magnitude (*i.e.*, to 10^{-2} a.u.) was found to yield insignificant changes to the results, suggesting that the third and higher order responses are negligible and that the molecules are in the linear response region. Alternatively, one can explicitly cancel the third-order contributions by carrying out extra single-point calculations within external electrostatic fields of doubled strength through[112]

$$\alpha_{ij} = \lim_{E_j \to 0} \frac{8[\mu_i(E_j) - \mu_i(-E_j)] - [\mu_i(2E_j) - \mu_i(-2E_j)]}{12E_j}, \quad (19)$$

which, as expected, was also found to have a negligible effect on the results.

Molecular Systems Studied

Altogether, 21 molecules were studied in this work, which are shown in Fig. 1, using a development version of Q-Chem 4.2.[113] For these molecules, we will begin by examining the atomic charges and the molecular dipole moments (as computed from these charges) as predicted by nine charge schemes (Mulliken, Löwdin, Becke, Hirshfeld, Hirshfeld-I, CM5, NPA, ESP, and CHELPG). When an external electrostatic field is applied (in any of the aforementioned 6 directions), one can compute the perturbed molecular dipole and atomic charges using any charge scheme, leading to the total molecular polarizability and its charge-fluctuating contribution (Eq. 13). With four charge schemes (Mulliken, Hirshfeld, Hirshfeld-I, and Becke), the induced-atomic-dipole contributions are also computed according to Eq. 18. There, Hirshfeld and Hirshfeld-I atomic dipoles are always computed using field-free atomic densities.

In addition, 12 dimers from the S22 database[114] were also studied, which are shown in Fig. 2. In these complexes, the monomers are interacting with each other through either hydrogen bonding or (parallel or T-shaped) π-π stacking. By calculating the amount of charge transferred between the monomers in each complex under the partition schemes, we investigated the significance of intermolecular charge transfer (CT), which might be useful guidance as to whether or not intermolecular CT can be neglected in the development of polarizable force fields.

In order to study the environment effect on the polarizability, a water pentamer, as shown in Fig. 3, was also considered. In this complex, a central water molecule is hydrogen bonded to four water molecules in a tetrahedral arrangement.

Results and Discussion

Atomic Charges and Molecular Dipoles

Basis Set and Functional Dependence of the charge definitions—The basis set dependence of the atomic multipoles (especially the monopoles) can be an important issue in force field development. To investigate this dependence, 9 atomic orbital basis sets were utilized in the calculation of the electronic structures of the model systems at the B3LYP[115] level of theory, including 7 Pople-style basis sets (6-31G(d), 6-31+G(d), 6-31+G(d,p), 6-311+G(d), 6-311+G(d,p), 6-311++G(d,p), 6-311++G(3df,3pd)) and 2 Dunning-style basis sets (cc-pVDZ and cc-pVTZ). The basis set dependence of the fitted charge for each definition was measured by

$$\chi = \sqrt{\frac{\sum_i \sum_j (Q_{ij} - \langle Q_i \rangle)^2}{\sum_i \sum_j 1}}, \quad (20)$$

where index i is for the atoms in all the molecules studied in this work and index j is for the basis sets. $\langle Q_i \rangle$ is the atomic charge for atom i averaged over all the basis sets. The results are shown in Table 1. Löwdin (χ = 0.1617 e) and Mulliken (χ = 0.1790 e) charges show the strongest basis set dependence, which is well-known in the community. Hirshfeld-I (χ = 0.0295 e), NPA (χ = 0.0234 e), and two ESP based charges, CHELPG (χ = 0.0253 e) and MK-ESP (χ = 0.0302 e), display basis set dependencies that are comparable among themselves, but are about one order of magnitude smaller than those of the Löwdin and Mulliken schemes and one order of magnitude larger than those of Becke (χ = 0.0031 e) and Hirshfeld/CM5 (χ = 0.0039 e) charges. Therefore, as far as basis set dependence is concerned, Löwdin and Mulliken charges are generally not ideal choices for the parameterization of force fields. Hirshfeld-I, NPA, CHELPG and MK-ESP are acceptable, while the best choices are Becke, Hirshfeld, and CM5 charges.

The density functional dependence ($\chi_{functional}$ in Table 1) is also calculated with Eq. 20 by comparing the fitted atomic charges from three density functional approximations, namely, B3LYP,[115] M06-2X,[116] and ωB97X-D,[117] with the 6-31G(d) basis set. Here j is the index for the functionals and $\langle Q_i \rangle$ is averaged over these three density functionals for atom i. The functional dependence is very weak with a root-mean-square-fluctuation (RMSF) of the atomic charges ranging from 0.0014 e for Becke and Hirshfeld/CM5 charges to 0.0067 e for Hirshfeld-I charges.

Molecular Dipoles: Molecular dipole moments, as computed from atomic charges (*i.e.*, the first term in Eq. 13), are shown in Table 2, where they are compared against the QM dipole moments computed from the electron density. We shall not attempt to compare them against experimental dipole moments because: (a) experimental dipole moments are not available for some molecules in our study; and (b) we have no reason to expect that the dipole

moments from atomic charges are more accurate than the underlying QM level of theory. Here are some observations from Table 2:

- The dipole moments from NPA charges show the largest positive deviation from the QM dipoles, with dipoles overestimated by 1.14 D in terms of the root-mean-square-deviation ($RMSD^b$, which only accounts for the scalar value of the dipole moments), and 35.6% in terms of the mean relative difference (MRD). This overestimation is more pronounced for molecules with small dipole moments, such as methyl ether, ethanol, methanol, and methanal.
- On the opposite end, due to the small charge values, the dipole moments from Hirshfeld charges are significantly lower than the QM values by 0.90 D in terms of the $RMSD^b$ and −31% in terms of the MRD.
- Mulliken ($RMSD^b$ = 0.69 D; MRD = 8.9%), Becke ($RMSD^b$ = 0.47 D; MRD = −6.5%), and Löwdin ($RMSD^b$ = 0.30 D; MRD = −3.9%) show increasingly improved dipole moments over NPA and Hirshfeld charges.
- With a correction to the systematic deviation in Hirshfeld charges, CM5 offers much improved dipole moments ($RMSD^b$ = 0.22 D; MRD = −6.2%).
- Hirshfeld-I, another scheme to improve upon Hirshfeld charges, also offers more accurate dipoles with a slightly lower $RMSD^b$ value of 0.18 D and a much better MRD value of −1.4%. This result is somewhat surprising because previous studies by other groups showed that the Hirshfeld-I scheme overestimates the atomic charges.[91,118]
- Out of all of the charge models, CHELPG and MK-ESP charges best reproduce the molecular dipole moments with a $RMSD^b$ value as small as 0.04 D and a MRD value of 1.1%. This is not surprising because these charges are fitted from the electrostatic potential on grid points around the molecules, which arise mainly from the molecular dipole moments (with smaller contributions from higher-order moments) for the 21 neutral molecules in this study.

The $RMSD^a$ values in Table 2, which are the RMSD of the vector difference between the computed and QM dipoles, can arise not only from a change in the magnitudes of the dipole moments but also from a change in their directions. Overall, $RMSD^a$ values correlate well with $RMSD^b$ values in this Table. For example, the $RMSD^a$ values are also small for the CHELPG and MK-ESP models, suggesting that these two models produce dipole moments with accurate values *and* To more clearly directions.

To more clearly measure the directionality, we collected the angles between the computed dipoles using various charge schemes and the QM dipoles in Table 3. The CHELPG and MK-ESP dipole moments align very well with the QM dipole moments, with an average angular deviation of 0.65°and 0.57°. Mulliken, Becke and NPA schemes change the orientation of the dipole moments the most, with an average angular deviation of 7.55°, 7.14°, and 6.78°, respectively. In between, four other schemes have moderate errors in the dipole angles: 4.24°(Hirshfeld), 3.43° (Löwdin), 2.87° (Hirshfeld-I), and 1.42° (CM5).

Therefore, as far as the dipole moment is concerned, CHELPG and MK-ESP charges appear to be good choices for developing force fields, while the Hirshfeld-I and CM5 charges might also be acceptable. Löwdin charges can be considered if one has to use a more conventional charge scheme.

Cross-Correlation among Charge Schemes—To further understand the various trends observed above for the computed molecular dipole moments, we plot the atomic charges derived from one scheme against those from another scheme in Fig. S1 and partially in Fig. 4. For each pair of schemes, the slope is calculated by minimizing a symmetric objective function $\chi^2=\sum_i\left(q_2^i/\sqrt{s}-\sqrt{s}q_1^i\right)^2$, which leads to $s=\sqrt{\sum_i(q_2^i)^2/\sum_i(q_1^i)^2}$. The slope values and correlations R^2 are listed in each panel in Fig. S1 and are also collected in Table 4. It is clear from these data that:

- The Löwdin charges correlate well with Mulliken charges (R^2 = 0.90), but a slope of 0.72 shows that Löwdin charges are smaller in many cases. In general, these two sets of charges correlate well with charges from other schemes, but the Mulliken charges tend to correlate much better with the ESP charges (CHELPG and MK-ESP) in terms of both R^2 values (0.94 and 0.95 versus 0.83 and 0.86) and slope values (1.02 and 1.07 versus 1.43 and 1.50).
- In general, the Becke charges do not correlate well with other charges, with R^2 values ranging from 0.54 with CHELPG charges to 0.75 with NPA charges. The only exception is the correlation between Becke charges and Löwdin charges (R^2=0.91 and slope=0.92).
- The Hirshfeld charges correlate reasonably well with those from other schemes (R^2 ranges from 0.84 with Löwdin to 0.90 with CHELPG), with the exception of Becke charges (R^2 = 0.60). On the other hand, Hirshfeld charges are consistently smaller than other charges, with a slope ranging from 0.27 against NPA charges and 0.50 against CM5 charges. This qualitatively explains the small dipole moments from Hirshfeld charges, which were shown above to have a −31.0% mean relative error.
- Both improvements to Hirshfeld charges, Hirshfeld-I and CM5, in general correlate well with other charges (again with the exception of Becke charges). Of the two, Hirshfeld-I correlates better with ESP charges in terms of the R^2 values (0.94 and 0.97 versus 0.90 and 0.90) and the slopes (0.90 and 0.94 versus 1.51 and 1.58).
- The NPA charges correlate reasonably well with most other schemes (R^2 values ranges from 0.89 with Hirshfeld to 0.98 with Mulliken charges), with the exception of Becke charges (R^2=0.75). NPA charges in general tend to be larger than other charges, with a slope of 1.15 against MK-ESP charges to 1.82 against CM5 charges. This is in qualitative agreement with the above observation that NPA dipole moments are on average 35.6% too large. Surprisingly, though, while NPA charges correlate well with Hirshfeld-I charges with R^2=0.94 and a slope of 1.08, the latter tend to better reproduce QM dipole moments.

- The best correlation occurs between two sets of ESP charges: CHELPG and MK-ESP. The R^2 value is 0.99 and the slope of CHELPG charges against MK-ESP charge is 0.95.

Intermolecular Charge Transfer—Charge transfer occurs naturally when there is a significant overlap of the electron density between two molecules. The amount of charge transferred from one monomer to another depends on the charge decomposition scheme, the basis set in use, and the underlying theoretical method. Table 5 lists the RMSF of the charge transferred as calculated at the B3LYP level of theory with the same basis sets used above. As in the case of individual monomers, the Löwdin decomposition scheme exhibits a significant basis set dependence (RMSF = 0.0187 e) and the Mulliken scheme displays an even more significant dependence (RMSF = 0.0418 e). On the other hand, other charge schemes display much weaker basis set dependence — RMSF ranges from 0.0023 e with Becke or NPA charges to 0.0069 e with MK-ESP charges, all below one hundredth of an electron.

B3LYP/6-31G(d) calculations were performed for the 12 dimers in Fig. 2, and the amount of charge transfer between the monomers is listed in Table 6. In general, less than 0.1 electron gets transferred between the monomers, with the only exception being the hydrogen bonded 2-pyridoxine/2-aminopyridine dimer for which MK-ESP scheme predicts a net transfer of 0.144 electron. Here are some observations:

- Despite its tendency to underestimate atomic charges (and thus molecular dipole moments), the Hirshfeld scheme produces the most significant charge transfer in 4 out of 12 complexes (benzene/water, T-shaped benzene/indole, phenol dimer, and water dimer; see boldfaced numbers in Table 6). As a result, the Hirshfeld scheme yields the most significant charge transfer (0.056 e) in terms of the mean unsigned average (MUA).
- Despite its tendency to overestimate atomic charges, the NPA scheme produces the least significant charge transfer in 9 out 12 complexes (see underlined numbers in Table 6). This is consistent with the localized picture in the NPA scheme. Consequently, its MUA is also the lowest (0.012 e).
- Except for 2-pyridoxine/2-aminopyridine and the hydrogen bonded adenine/thymine complex, the Becke scheme predicts an opposite direction for the charge transfer when compared against other schemes. It also leads to the most significant mean signed average (MSA) of charge transfer (−0.011 e) among all of the charge schemes.
- In most of the dimers containing benzene (benzene/ammonia, T-shaped benzene dimer, benzene/HCN, benzene/methane, benzene/water, T-shaped benzene/indole), in which benzene interacts with the other monomer through its delocalized π-electrons, the benzene plays the role of electron donor. The only exception is the stacked benzene/indole complex. With the Hirshfeld-I scheme, the amount of electron charges transferred out of benzene depends on the electronegativity of the other monomer. HCN attracts the largest amount of electron density from benzene, followed by benzene and water.

- Similar amounts of charge transfer can also be observed for the phenol dimer and water dimer. With most charge schemes, the amount of charge transfer becomes significantly lower in the 2-pyridoxine/2-aminopyridine complex and the hydrogen bonded adenine/thymine dimer, where each monomer functions as both a hydrogen bond donor and an acceptor. For these two complexes, we note that the ESP schemes (CHELPG and MK-ESP) predict quite significant charge transfers, which likely only reflects the deficiencies of these ESP-based schemes on systems with buried atoms.

Decomposition of Static Molecular Polarizabilities

Molecular Polarizability—After diagonalizing the static molecular polarizability tensor (computed via finite differences), the anisotropy of the polarizability can be measured by[119]

$$\Delta\alpha=\frac{\sqrt{\frac{1}{2}\left[(\tilde{\alpha}_{xx}-\tilde{\alpha}_{yy})^2+(\tilde{\alpha}_{yy}-\tilde{\alpha}_{zz})^2+(\tilde{\alpha}_{zz}-\tilde{\alpha}_{xx})^2\right]}}{\frac{1}{3}(\tilde{\alpha}_{xx}+\tilde{\alpha}_{yy}+\tilde{\alpha}_{zz})}, \quad (21)$$

where $\tilde{\alpha}_{xx}$, $\tilde{\alpha}_{yy}$ and $\tilde{\alpha}_{zz}$ are the real part of the three components of the diagonalized polarizability tensor $\tilde{\alpha}$. The results calculated at the B3LYP/6-31G(d) level of theory are depicted in Fig. 5 and are also listed in Table 7. Clearly, the anisotropies are quite different among these molecules. Due to their high point group symmetry (T_d), the anisotropies for neopentane and methane are exactly zero. On the other hand, planar molecules can have large anisotropies, because the in-plane polarizability is much larger than the out-of-plane polarizability. In fact, adenine, benzene, formamide, indole, methanal, pNA, mNA, thymine, uracil, and water all have high levels of anisotropy between 0.698 (formic acid) and 1.020 (indole). Dodecahexene, whose polarizability aligns mainly along the molecular axis, has an even larger anisotropy of 2.061.

Contribution from Fluctuating Charges—The ratio of the charge fluctuation contributions to the total static molecular polarizability can be calculated as

$$s=\frac{\mathbf{Tr}\left(\alpha^{FC}\right)}{\mathbf{Tr}\left(\alpha\right)}, \quad (22)$$

where **Tr** is the trace operator and the values of *s* are shown in Table 8. From this table, it is clear that charge fluctuations contribute substantially to the molecular polarization, with its ratio ranging from 59.94% with the Hirshfeld scheme to 96.25% with the Mulliken scheme. Sometimes, especially with the Mulliken scheme, the ratio of the FC contribution can be over 100%, which simply means that the sum of induced atomic dipoles (*i.e.*, the second term in Eq. 15) has the opposite direction to the FC contribution (*i.e.*, the first term in Eq. 15), making the net induced dipole smaller than the FC contribution. The Hirshfeld-I charge model has very large FC contributions, with the smallest being for methanal (69.44%). This result indicates that it might be problematic to neglect charge transfer effects in polarizable force fields, which would require rather large atomic polarizabilities (and thus induced

atomic dipoles) to mimic the significant amount of charge migration under an external perturbation.

Atomic Polarizability—When a molecule is subjected to an external electrostatic potential, the induced dipole moment on each atom can be calculated with the Mulliken, Hirshfeld, Hirshfeld-I, and Becke partition schemes (*i.e.*, the second term in Eq. 15), and the corresponding atomic polarizability $\left(\hat{\boldsymbol{\alpha}}^{IAD}\right)$ can be calculated with Eq. 18. In general, $\left(\hat{\boldsymbol{\alpha}}^{IAD}\right)$ is a nonsymmetric 3 × 3 matrix, and its diagonalization leads to three principal polarizability components, which are not necessarily perpendicular to each other.

The three principal polarizability components were obtained under the Hirshfeld-I partitioning scheme for eight molecules, and the results are shown in Fig. 6. Overall, both the magnitudes and directions of the atomic polarizability components appear to be sensitive to the local connectivity. Here are some observations for different atom types:

- Nonpolar hydrogen atoms (those connected to carbon atoms). The three principal polarizabilies of the hydrogen atoms are (0.410, 0.410, 0.768) for methane and (0.496, 0.500, 0.977) for benzene, with the largest components (0.768 or 0.977) pointing along the C-H bond in both molecules. For methanol, the three components are (0.422, 0.501, 0.749) or (0.492, 0.524, 0.945), again with the largest component along the C-H bond. It is somewhat disturbing that the two methyl hydrogen atoms closer to the hydroxyl group appear to be significantly more polarizable, because all charge models in this work predict small variations in the charges on the three hydrogen atoms (0.0477, 0.0477, and 0.0807 e under the Hirshfeld-I scheme and 0.0160, 0.0160, and 0.0805 e under the MK-ESP scheme). The atomic polarizabilities of the hydrogen atoms connected to carbonyl carbon atoms also vary significantly: the three components are (0.509, 0.673, 1.134) for methanal, with a rather large component (1.134) along the C-H bond; while the atomic polarizabilities are more isotropic for nonpolar hydrogens in formamide and formic acid: (0.579, 0.706, 0.741) for formamide, and (0.539, 0.679, 0.696) for formic acid, where the smallest components (0.579 or 0.539) point nearly along the C-H bond.
- Polar hydrogen atoms (those connected to oxygen or nitrogen atoms). Compared to nonpolar hydrogen atoms, whose atomic polarizabilities range from 0.410 to 1.134, the polar hydrogen atoms have smaller atomic polarizabilities, mostly likely because these hydrogen atoms lose a significant fraction of their electrons to their neighboring atoms and thus become less polarizable. The three components are (0.137, 0.137, 0.250) for water, with the largest component (0.250) along the direction perpendicular to the molecular plane. The hydroxyl hydrogen in formic acid has a more isotropic atomic polarizability of (0.158, 0.158, 0.234), with the largest component also perpendicular to the molecular plane; in contrast, methanol has a less isotropic atomic polarizability of (0.069, 0.210, 0.317), with the largest component (0.317) within the C-O-H plane and nearly perpendicular to the O-H bond. Compared to hydroxyl hydrogens, atomic polarizabilities of amine hydrogen

atoms are similar in magnitude but are more isotropic: (0.233, 0.274, 0.274) for ammonia, and (0.241, 0.270, 0.270) or (0.237, 0.248, 0.270) for the two amine hydrogens in formamide.

- **Carbon atoms.** As expected, the atomic polarizability of the carbon atom in methane is perfectly isotropic with a value of 0.761 along all directions. Carbon atoms in benzene, on other hand, are extremely anisotropic: they are most polarizable perpendicular to the molecular plane with a component of 3.002 (suggesting that the π-electrons are most polarizable); and the value is 0.589 along the six-membered ring, and most interestingly, the polarizability is −0.464 along C-H bonds. In other words, an electric field along the C-H bond will generate an opposing response. The atomic polarizabilities of carbonyl carbon atoms are even more anisotropic with two negative components: (−0.956, −0.235, 2.776) for formamide, (−0.897, −0.297, 3.020) for formic acid, and (−0.687, −0.501, 3.288) for methanal, with the largest component (2.776 or 3.020 or 3.288) perpendicular to the molecular plane (again suggesting that the π-electrons are most polarizable), and the negative components lie in the molecular plane.

- **Oxygen atoms.** Carbonyl oxygens have very large atomic polarizabilities: (1.372, 1.908, 2.639) for formamide; (1.240, 2.007, 2.611) for formic acid; (1.046, 1.756, 2.456) for methanal, with the largest components (2.639 or 2.611 or 2.456) all perpendicular to the molecular plane (*i.e.*, π-electrons are most polarizable). But even the smallest component, which lies along the C=O bond, is quite significant (1.372 or 1.240 or 1.046). Hydroxyl oxygen atoms also have large atomic polarizabilities: (0.115, 1.848, 2.279) for formic acid, (0.171, 1.873, 1.931) for methanol, and (0.461, 0.544, 2.338) for water, all with a large component of polarizability (2.279 or 1.873 or 2.338) lying perpendicular to the plane formed by the oxygen atom and its two neighbors. The component that bifurcates its neighboring atoms has a large fluctuation (1.848 or 1.931 or 0.544) among the three molecules. Meanwhile, the third component is much smaller in magnitude.

  To further investigate the transferability of atomic polarizabilities, the principal polarizability components of hydroxyl oxygen atoms and carbonyl oxygen atoms appearing in all of the 21 molecules are projected into the atomic local frame[120] and are plotted in Fig. 7. For hydroxyl oxygen atoms, the *z* component of the polarizability, *i.e.*, the component perpendicular to the plane formed by the oxygen atom and its neighbors, is very consistent in all the molecules. But the other two components are scattered and have large fluctuations in magnitude. For the carbonyl oxygen atom, all of the three components vary significantly from molecule to molecule. As such, this figure demonstrates some degree of transferability for the computed atomic polarizabilities.

- **Nitrogen atoms.** The dominant component of the atomic polarizability (1.590) of the nitrogen atom in ammonia lies along the axis of C_3 symmetry. The other two components are degenerate and the magnitude (0.751) is about one half of the first component. On other hand, the nitrogen atom in formamide has much larger component (3.072) of polarizability perpendicular to the H-N-C plane. The second

component (1.234) points along the N-C bond. And the third one has a small negative value (−0.299).

Overall, with the exceptions of the carbon atom in methane (which is in a high symmetry local environment) and the hydrogen atoms in hydroxyl groups, the atomic polarizabilities as computed in this work are rather anisotropic. As an extreme case, the three components of the atomic polarizability of the hydroxyl oxygen atom in formic acid can differ in magnitude by a factor of 20 (*i.e.*, 0.115 versus 2.279). Some components can even be negative, such as for benzene carbon, carbonyl carbon, and amide nitrogen atom. The importance of anisotropy in the polarizability has also been investigated several times before[121–123] and a computationally feasible solution has also been presented.[124]

As a further investigation of the transferability of computed atomic polarizabilities (and thus their applicability in extended systems), a calculation on the water pentamer[125] (shown in Fig. 3) was performed. The central water molecule is embedded in an inhomogeneous electrostatic environment generated by the four other water molecules. Marenich *et al.* noticed that the total polarizability (including both the charge transfer term and local deformation of electron density) of buried atoms can be reduced or quenched by its surrounding atoms.[126] We observe the same for this water pentamer under the Hirshfeld partition scheme. Table 9 shows that the polarizability of the oxygen atom in the central water molecule is more isotropic and is around 1.61 a.u., while the atomic polarizability components of the oxygen atoms in the other water molecules are less isotropic and are in the range from 1.86 to 2.23 a.u.. However, Hirshfeld-I analysis indicates that the average atomic polarizabilities of the oxygen atom in the central water molecule (1.68) are larger than those of the surrounding oxygen atoms: 1.19 for the two hydrogen bond acceptor water molecules; and 1.36 for the two hydrogen bond donor water molecules. Besides, these water molecules differ from the gas-phase water molecule (see Fig. 6) in terms of their atomic polarizability with a varying degree: gas (1.11) < acceptor (1.19) < donor (1.36) < central (1.68).

Conclusions

The static molecular polarizability, which is the response of a molecule to an external electric field, was computed in this work for 21 small molecules using density functional theory and a finite-difference scheme. Altogether, nine charge population schemes (Löwdin, Mulliken, Becke, Hirshfeld, Hirshfeld-I, NPA, CM5, CHELPG, MK-ESP) were employed to compute the charge fluctuation contribution to the molecular polarizability. Four schemes (Mulliken, Becke, Hirshfeld, Hirshfeld-I), for which atomic electronic densities are well-defined, can also yield the induced dipole contributions from each atom to the molecular polarizability. Our results show that:

- The fluctuating charge contribution to the molecular polarizability is found to be rather significant with all nine charge schemes, with its ratio ranging from 59.9% with the Hirshfeld or CM5 scheme to 96.2% with the Mulliken scheme for the 21 small molecules included in this study.

- The atomic polarizabilities, as computed from the induced atomic dipoles for 8 small molecules using the Hirshfeld-I scheme, are clearly anisotropic for the vast majority of atoms. For example, the out-of-plane polarizability of benzene carbon atoms or carbonyl carbon atoms can be significantly larger than the other components, meaning that π electrons are more polarizable than other electrons. Some components of the computed atomic polarizabilities are even negative.

This suggests to us that (a) more emphasis probably should be placed on the charge fluctuating terms in future polarizable force field development; (b) an anisotropic polarizability might be more suitable than an isotropic one in polarizable force fields based entirely or partially on the induced atomic dipoles.

On the other hand, this work has several limitations:

- This work does not address the Pauli repulsion or dispersion effects, which are strongly coupled to the polarization effect (the main focus of this work) in condensed-phase simulations. We note that Pauli repulsion has been included in a quantum mechanical manner in *ab initio*-derived force fields such as the effective fragment potential.[127]
- While the significance of charge fluctuations within the molecules is clearly demonstrated, this work does not provide any new route forward to account for the charge fluctuation effect via a force field.
- Arguably in the computation of atomic polarizabilities using Eq. 18, one can use the effective electric field on individual atoms instead of the applied external field.
- The atomic polarizabilities as computed using Eq. 18 showed some, albeit limited, transferability across molecules. Therefore, more work is needed to turn such observations into practical force fields.

For the last point, one potential approach to move forward is to extend this study to many more compounds and gain a more complete understanding of atomic polarizabilities (as computed from the induced atomic dipoles), especially their anisotropy. Then one could use that understanding to develop a proper parameterization scheme and, since the polarizability in condensed phase (even in water pentamer) can significantly differ from that in the gas phase, [128–131] use QM/MM calculations to fit anisotropic atomic polarizabilities in a self-consistent fashion.[132,133]

During the course of decomposing the molecular polarizabilities, we have also reconfirmed several known facts about atomic charges:

- Mulliken and Löwdin charges have a stronger basis set dependence than other charges. Hirshfeld-I, NPA, CHELPG, and MK-ESP charges show moderate basis-set dependence. Becke, Hirshfeld and CM5 are the least basis-set dependent charge schemes.
- Compared to basis-set dependence, the dependence on the density functional approximation is weaker but still not negligible.

- Two ESP-based schemes, CHELPG and MK-ESP, best reproduce the dipole moments as computed from the quantum mechanical electron density. Hirshfeld charges, which are systematically smaller than other charges, lead to underestimated molecular dipole moments. As a significant improvement, the Hirshfeld-I scheme well reproduces both the magnitudes and the directions of the molecular dipole moments. NPA, on other hand, yields significantly overestimated molecular dipole moments. Löwdin and Becke charge schemes perform better than Mulliken charge scheme, but less well than Hirshfeld-I, CHELPG, and MK-ESP schemes.
- For a subset of 12 molecular complexes from the S22 database, the amount of charge transfer between the two monomers generally falls between 0.01 and 0.1 e, but these amounts are noticeably dependent on the charge scheme. Surprisingly, Hirshfeld charges, which are relatively small compared to other charges, predict the largest amount of charge transfer for 4 out of 12 complexes and also the largest mean unsigned average for the 12 complexes. On the other hand, NPA charges, which tend to be larger than other charges, predict the smallest amount of charge transfer for 9 out of 12 complexes and also the smallest average across the 12 complexes.

We note that the energy stabilization associated with charge transfer has been investigated for the water dimer,[134,135] but its effect in other complexes has yet to be investigated systematically. If the charge transfer interaction energies are shown to be substantial, it will be even more desirable to include explicit charge fluctuation terms in future polarizable force fields.

Supplementary Material

Refer to Web version on PubMed Central for supplementary material.

Acknowledgement

YM is supported by the National Natural Science Foundation of China (Grant No. 21173082) and the China Scholarship Council (Grant No. 201208310344). YS is supported by NIH grant GM096678-02 and DOE grant No. DE-SC0011297. ACS, FCP and BRB are supported by the Intramural Research Program of the NIH, NHLBI. Computational resources and services used in this work were partially provided by the LoBoS cluster of the National Institutes of Health.

Several charge partitioning schemes in Q-Chem were employed in this study, and YS thanks the Troy van Voorhis group for their implementation of Becke and Hirshfeld charges, Drs. Alek Marenich and Don Truhlar for the implementation of CM5 charges, Dr. Eric Glendening for the implementation of natural population analysis, and the John Herbert group for the implementation of CHELPG charges. YS also thanks Dr. Ramkumar Rajamani for helpful discussions on Hirshfeld charges, Mr. Ka Un Lao and Dr. John Herbert for helpful discussions on iterative Hirshfeld charges, and Dr. Qin Wu for discussions about Becke charges.

References

(1). Shea J-E. Simulations Pave the Way for Exploring New Frontiers in the Biological Sciences. J. Phys. Chem. Lett. 2014; 5:1783–1784.

(2). van Maaren PJ, van der Spoel D. Molecular Dynamics Simulations of Water with Novel Shell-Model Potentials. J. Phys. Chem. B. 2001; 105:2618–2626.

(3). Harder E, Anisimov VM, Whitfield T, MacKerell AD, Roux B. Understanding the Dielectric Properties of Liquid Amides from a Polarizable Force Field. J. Phys. Chem. B. 2008; 112:3509–3521. [PubMed: 18302362]

(4). Jorgensen WL. Special Issue on Polarization. J. Chem. Theory Comput. 2007; 3:1877–1877.

(5). Lu Z, Zhang Y. Interfacing ab Initio Quantum Mechanical Method with Classical Drude Osillator Polarizable Model for Molecular Dynamics Simulation of Chemical Reactions. J. Chem. Theory Comput. 2008; 4:1237–1248. [PubMed: 19221605]

(6). Wang L-P, Van Voorhis T. A Polarizable QM/MM Explicit Solvent Model for Computational Electrochemistry in Water. J. Chem. Theory Comput. 2012; 8:610–617.

(7). Boulanger E, Thiel W. Solvent Boundary Potentials for Hybrid QM/MM Computations Using Classical Drude Oscillators: A Fully Polarizable Model. J. Chem. Theory Comput. 2012; 8:4527–4538.

(8). Halgren TA, Damm W. Polarizable Force Fields. Curr. Opin. Struc. Biol. 2001; 11:236–242.

(9). Rick, SW.; Stuart, SJ. Reviews in Computational Chemistry. John Wiley & Sons, Inc.; 2003. p. 89-146.

(10). Yu HB, van Gunsteren WF. Accounting for Polarization in Molecular Simulation. Comput. Phys. Commun. 2005; 172:69–85.

(11). Lopes P, Roux B, MacKerell AD Jr. Molecular Modeling and Dynamics Studies with Explicit Inclusion of Electronic Polarizability: Theory and Applications. Theor. Chem. Acc. 2009; 124:11–28. [PubMed: 20577578]

(12). Demerdash O, Yap E-H, Head-Gordon T. Advanced Potential Energy Surfaces for Condensed Phase Simulation. Annu. Rev. Phys. Chem. 2014; 65:149–174. [PubMed: 24328448]

(13). Gasteiger J, Marsili M. A New Model for Calculating Atomic Charges in Molecules. Tetrahedron Lett. 1978; 19:3181–3184.

(14). Rappe AK, Goddard WA. Charge Equilibration for Molecular Dynamics Simulations. J. Phys. Chem. 1991; 95:3358–3363.

(15). Rick SW, Stuart SJ, Berne BJ. Dynamical Fluctuating Charge Force Fields: Application to Liquid Water. J. Chem. Phys. 1994; 101:6141–6156.

(16). Kaminski GA, Stern HA, Berne BJ, Friesner RA, Cao YX, Murphy RB, Zhou R, Halgren TA. Development of a Polarizable Force Field for Proteins via ab initio Quantum Chemistry: First Generation Model and Gas Phase Tests. J. Comput. Chem. 2002; 23:1515–1531. [PubMed: 12395421]

(17). Patel S, Brooks CL. CHARMM Fluctuating Charge Force Field for Proteins: I Parameterization and Application to Bulk Organic Liquid Simulations. J. Comput. Chem. 2004; 25:1–16. [PubMed: 14634989]

(18). Chen J, Martínez TJ. QTPIE: Charge Transfer with Polarization Current Equalization. A Fluctuating Charge Model with Correct Asymptotics. Chem. Phys. Lett. 2007; 438:315.

(19). Warshel A, Levitt M. Theoretical Studies of Enzymic Reactions: Dielectric, Electrostatic and Steric Stabilization of the Carbonium Ion in the Reaction of Lysozyme. J. Mol. Biol. 1976; 103:227–249. [PubMed: 985660]

(20). Vesely FJ. N-Particle Dynamics of Polarizable Stockmayer-Type Molecules. J. Comput. Phys. 1977; 24:361–371.

(21). Piquemal J-P, Williams-Hubbard B, Fey N, Deeth RJ, Gresh N, Giessner-Prettre C. Inclusion of the Ligand Field Contribution in a Polarizable Molecular Mechanics: SIBFA-LF. J. Comput. Chem. 2003; 24:1963–1970. [PubMed: 14531050]

(22). Xie W, Pu J, MacKerell AD, Gao J. Development of a Polarizable Intermolecular Potential Function (PIPF) for Liquid Amides and Alkanes. J. Chem. Theory Comput. 2007; 3:1878–1889. [PubMed: 18958290]

(23). Jorgensen WL, Jensen KP, Alexandrova AN. Polarization Effects for Hydrogen-Bonded Complexes of Substituted Phenols with Water and Chloride Ion. J. Chem. Theory Comput. 2007; 3:1987–1992. [PubMed: 21132092]

(24). Wang J, Cieplak P, Li J, Hou T, Luo R, Duan Y. Development of Polarizable Models for Molecular Mechanical Calculations I: Parameterization of Atomic Polarizability. J. Phys. Chem. B. 2011; 115:3091–3099. [PubMed: 21391553]

(25). Ren P, Ponder JW. Polarizable Atomic Multipole Water Model for Molecular Mechanics Simulation. J. Phys. Chem. B. 2003; 107:5933–5947.

(26). Ponder JW, Wu C, Ren P, Pande VS, Chodera JD, Schnieders MJ, Haque I, Mobley DL, Lambrecht DS, DiStasio RA, et al. Current Status of the AMOEBA Polarizable Force Field. J. Phys. Chem. B. 2010; 114:2549–2564. [PubMed: 20136072]

(27). Shi Y, Xia Z, Zhang J, Best R, Wu C, Ponder JW, Ren P. Polarizable Atomic Multipole-Based AMOEBA Force Field for Proteins. J. Chem. Theory Comput. 2013; 9:4046–4063. [PubMed: 24163642]

(28). Lamoureux G, Roux B. Modeling Induced Polarization with Classical Drude Oscillators: Theory and Molecular Dynamics Simulation Algorithm. J. Chem. Phys. 2003; 119:3025–3039.

(29). Harder E, Anisimov VM, Vorobyov IV, Lopes PEM, Noskov SY, MacKerell AD, Roux B. Atomic Level Anisotropy in the Electrostatic Modeling of Lone Pairs for a Polarizable Force Field Based on the Classical Drude Oscillator. J. Chem. Theory Comput. 2006; 2:1587–1597.

(30). Lamoureux G, Harder E, Vorobyov IV, Roux B, MacKerell AD Jr. A Polarizable Model of Water for Molecular Dynamics Simulations of Biomolecules. Chem. Phys. Lett. 2006; 418:245–249.

(31). Geerke DP, van Gunsteren WF. On the Calculation of Atomic Forces in Classical Simulation Using the Charge-on-Spring Method To Explicitly Treat Electronic Polarization. J. Chem. Theory Comput. 2007; 3:2128–2137.

(32). Jiang W, Hardy DJ, Phillips JC, MacKerell AD, Schulten K, Roux B. High-Performance Scalable Molecular Dynamics Simulations of a Polarizable Force Field Based on Classical Drude Oscillators in NAMD. J. Phys. Chem. Lett. 2011; 2:87–92. [PubMed: 21572567]

(33). Yu W, Lopes PEM, Roux B, MacKerell AD. Six-Site Polarizable Model of Water Based on the Classical Drude Oscillator. J. Chem. Phys. 2013; 138:034508. [PubMed: 23343286]

(34). Lopes PEM, Huang J, Shim J, Luo Y, Li H, Roux B, MacKerell AD. Polarizable Force Field for Peptides and Proteins Based on the Classical Drude Oscillator. J. Chem. Theory Comput. 2013; 9:5430–5449. [PubMed: 24459460]

(35). Stern HA, Kaminski GA, Banks JL, Zhou R, Berne BJ, Friesner RA. Fluctuating Charge, Polarizable Dipole, and Combined Models: Parameterization from ab Initio Quantum Chemistry. J. Phys. Chem. B. 1999; 103:4730–4737.

(36). Stern HA, Rittner F, Berne BJ, Friesner RA. Combined Fluctuating Charge and Polarizable Dipole Models: Application to a Five-Site Water Potential Function. J. Chem. Phys. 2001; 115:2237–2251.

(37). Salomon-Ferrer R, Case DA, Walker RC. An Overview of the Amber Biomolecular Simulation Package. WIREs Comput. Mol. Sci. 2013; 3:198–210.

(38). Brooks BR, Brooks CL, Mackerell AD, Nilsson L, Petrella RJ, Roux B, Won Y, Archontis G, Bartels C, Boresch S, et al. CHARMM: The Biomolecular Simulation Program. J. Comput. Chem. 2009; 30:1545–1614. [PubMed: 19444816]

(39). Phillips JC, Braun R, Wang W, Gumbart J, Tajkhorshid E, Villa E, Chipot C, Skeel RD, Kal L, Schulten K. Scalable Molecular Dynamics with NAMD. J. Comput. Chem. 2005; 26:1781–1802. [PubMed: 16222654]

(40). Hess B, Kutzner C, van der Spoel D, Lindahl E. GROMACS 4: Algorithms for Highly Efficient, Load-Balanced, and Scalable Molecular Simulation. J. Chem. Theory Comput. 2008; 4:435–447.

(41). Thole BT. Molecular Polarizabilities Calculated with a Modified Dipole Interaction. Chem. Phys. 1981; 59:341–350.

(42). Ren P, Ponder JW. Consistent Treatment of Inter- and Intramolecular Polarization in Molecular Mechanics Calculations. J. Comput. Chem. 2002; 23:1497–1506. [PubMed: 12395419]

(43). Drude, P. The Theory Of Optics. Kessinger Publishing, LLC.; 1902.

(44). Born, M.; Huang, K. Dynamic Theory of Crystal Lattices. Oxford University Press; Oxford, UK: 1954.

(45). Straatsma TP, McCammon JA. Molecular Dynamics Simulations with Interaction Potentials Including Polarization Development of a Noniterative Method and Application to Water. Mol. Simul. 1990; 5:181–192.

(46). Baker C, MacKerell J, Alexander D. Polarizability Rescaling and Atom-Based Thole Scaling in the CHARMM Drude Polarizable Force Field for Ethers. J. Mol. Model. 2010; 16:567–576. [PubMed: 19705172]

(47). Woodcock HL, Hodošček M, Gilbert ATB, Gill PMW, Schaefer HF, Brooks BR. Interfacing Q-Chem and CHARMM to Perform QM/MM Reaction Path Calculations. J. Comput. Chem. 2007; 28:1485–1502. [PubMed: 17334987]

(48). Boulanger E, Thiel W. Toward QM/MM Simulation of Enzymatic Reactions with the Drude Oscillator Polarizable Force Field. J. Chem. Theory Comput. 2014; 10:1795–1809.

(49). MacKerell, AD.; Brooks, B.; Brooks, CL.; Nilsson, L.; Roux, B.; Won, Y.; Karplus, M. Encyclopedia of Computational Chemistry. John Wiley & Sons, Ltd; 2002.

(50). Vanommeslaeghe K, Hatcher E, Acharya C, Kundu S, Zhong S, Shim J, Darian E, Guvench O, Lopes P, Vorobyov I, et al. CHARMM General Force Field: A Force Field for Drug-Like Molecules Compatible with the CHARMM All-Atom Additive Biological Force Fields. J. Comput. Chem. 2010; 31:671–690. [PubMed: 19575467]

(51). Duan Y, Wu C, Chowdhury S, Lee MC, Xiong G, Zhang W, Yang R, Cieplak P, Luo R, Lee T, et al. A Point-Charge Force Field for Molecular Mechanics Simulations of Proteins Based on Condensed-Phase Quantum Mechanical Calculations. J. Comput. Chem. 2003; 24:1999–2012. [PubMed: 14531054]

(52). Jorgensen WL, Maxwell DS, Tirado-Rives J. Development and Testing of the OPLS All-Atom Force Field on Conformational Energetics and Properties of Organic Liquids. J. Am. Chem. Soc. 1996; 118:11225–11236.

(53). Akin-Ojo O, Song Y, Wang F. Developing ab initio Quality Force Fields from Condensed Phase Quantum-Mechanics/Molecular-Mechanics Calculations Through the Adaptive Force Matching Method. J. Chem. Phys. 2008; 129:064108. [PubMed: 18715052]

(54). Roy Kimura S, Rajamani R, Langley DR. Quantum Polarized Fluctuating Charge Model: A Practical Method to Include Ligand Polarizability in Biomolecular Simulations. J. Chem. Phys. 2011; 135:231101. [PubMed: 22191857]

(55). Cerutti DS, Rice JE, Swope WC, Case DA. Derivation of Fixed Partial Charges for Amino Acids Accommodating a Specific Water Model and Implicit Polarization. J. Phys. Chem. B. 2013; 117:2328–2338. [PubMed: 23379664]

(56). Ji C, Mei Y, Zhang JZH. Developing Polarized Protein-Specific Charges for Protein Dynamics: MD Free Energy Calculation of pKa Shifts for Asp26/Asp20 in Thioredoxin. Biophys. J. 2008; 95:1080–1088. [PubMed: 18645195]

(57). Lee LP, Cole DJ, Skylaris C-K, Jorgensen WL, Payne MC. Polarized Protein-Specific Charges from Atoms-in-Molecule Electron Density Partitioning. J. Chem. Theory Comput. 2013; 9:2981–2991. [PubMed: 23894231]

(58). Leontyev IV, Stuchebrukhov AA. Polarizable Molecular Interactions in Condensed Phase and Their Equivalent Nonpolarizable Models. J. Chem. Phys. 2014; 141:014103. [PubMed: 25005273]

(59). Leontyev I, Stuchebrukhov A. Accounting for Electronic Polarization in Non-Polarizable Force Fields. Phys. Chem. Chem. Phys. 2011; 13:2613–2626. [PubMed: 21212894]

(60). Duan LL, Mei Y, Zhang D, Zhang QG, Zhang JZH. Folding of a Helix at Room Temperature is Critically Aided by Electrostatic Polarization of Intraprotein Hydrogen Bonds. J. Am. Chem. Soc. 2010; 132:11159–11164. [PubMed: 20698682]

(61). Söderhjelm P, Öhrn A, Ryde U, Karlström G. Accuracy of Typical Approximations in Classical Models of Intermolecular Polarization. J. Chem. Phys. 2008; 128:014102. [PubMed: 18190180]

(62). Wang L-P, Head-Gordon T, Ponder JW, Ren P, Chodera JD, Eastman PK, Martinez TJ, Pande VS. Systematic Improvement of a Classical Molecular Model of Water. J. Phys. Chem. B. 2013; 117:9956–9972. [PubMed: 23750713]

(63). Stone AJ, Misquitta AJ. Atom-atom Potentials from ab initio Calculations. Int. Rev. Phys. Chem. 2007; 26:193–222.

(64). Elking D, Darden T, Woods RJ. Gaussian Induced Dipole Polarization Model. J. Comput. Chem. 2007; 28:1261–1274. [PubMed: 17299773]

(65). Woo Kim H, Rhee YM. Molecule-Specific Determination of Atomic Polarizabilities with the Polarizable Atomic Multipole Model. J. Comput. Chem. 2012; 33:1662–1672. [PubMed: 22565616]

(66). Sodt A, Mei Y, König G, Tao P, Ryan S, Brooks B, Shao Y. Multiple Environment Single System Quantum Mechanical/Molecular Mechanical (MESS-QM/MM) Calculations. I. Estimation of Polarization Energies. J. Phys. Chem. A. 2014; 119:1511–1523. [PubMed: 25321186]

(67). Storer J, Giesen D, Cramer C, Truhlar DG. Class IV Charge Models: A New Semiempirical Approach in Quantum Chemistry. J. Comput. Aid. Mol. Des. 1995; 9:87–110.

(68). Marenich AV, Jerome SV, Cramer CJ, Truhlar DG. Charge Model 5: An Extension of Hirshfeld Population Analysis for the Accurate Description of Molecular Interactions in Gaseous and Condensed Phases. J. Chem. Theory Comput. 2012; 8:527–541.

(69). Gasteiger J, Marsili M. Iterative Partial Equalization of Orbital Electronegativity–Rapid Access to Atomic Charges. Tetrahedron. 1980; 36:3219–3228.

(70). Mortier WJ, Van Genechten K, Gasteiger J. Electronegativity Equalization: Application and Parametrization. J. Am. Chem. Soc. 1985; 107:829–835.

(71). Coppens P. Electron Density from X-Ray Diffraction. Annu. Rev. Phys. Chem. 1992; 43:663–692.

(72). Mulliken RS. Electronic Population Analysis on LCAO-MO Molecular Wave Functions. I. J. Chem. Phys. 1955; 23:1833–1840.

(73). Mulliken RS. Criteria for the Construction of Good Self-Consistent-Field Molecular Orbital Wave Functions, and the Significance of LCAO-MO Population Analysis. J. Chem. Phys. 1962; 36:3428–3439.

(74). Löwdin P-O. On the Non-Orthogonality Problem Connected with the Use of Atomic Wave Functions in the Theory of Molecules and Crystals. J. Chem. Phys. 1950; 18:365–375.

(75). Baker J. Classical Chemical Concepts from ab initio SCF Calculations. Theor. Chim. Acta. 1985; 68:221–229.

(76). Bader RFW. A Quantum Theory of Molecular Structure and Its Applications. Chem. Rev. 1991; 91:893–928.

(77). Reed AE, Weinstock RB, Weinhold F. Natural Population Analysis. J. Chem. Phys. 1985; 83:735–746.

(78). Reed AE, Curtiss LA, Weinhold F. Intermolecular Interactions from a Natural Bond Orbital, Donor-Acceptor Viewpoint. Chem. Rev. 1988; 88:899–926.

(79). Hirshfeld F. Bonded-Atom Fragments for Describing Molecular Charge Densities. Theor. Chim. Acta. 1977; 44:129–138.

(80). Bultinck P, Van Alsenoy C, Ayers PW, Carbó-Dorca R. Critical Analysis and Extension of the Hirshfeld Atoms in Molecules. J. Chem. Phys. 2007; 126:144111. [PubMed: 17444705]

(81). Becke AD. A Multicenter Numerical Integration Scheme for Polyatomic Molecules. J. Chem. Phys. 1988; 88:2547–2553.

(82). Davidson E, Chakravorty S. A Test of the Hirshfeld Definition of Atomic Charges and Moments. Theor. Chim. Acta. 1992; 83:319–330.

(83). Geldof D, Krishtal A, Blockhuys F, Van Alsenoy C. An Extension of the Hirshfeld Method to Open Shell Systems Using Fractional Occupations. J. Chem. Theory Comput. 2011; 7:1328–1335.

(84). Geldof D, Krishtal A, Blockhuys F, Van Alsenoy C. FOHI-D: An Iterative Hirshfeld Procedure Including Atomic Dipoles. J. Chem. Phys. 2014; 140:144104. [PubMed: 24735285]

(85). Lillestolen TC, Wheatley RJ. Atomic Charge Densities Generated Using an Iterative Stockholder Procedure. J. Chem. Phys. 2009; 131:144101. [PubMed: 19831427]

(86). Misquitta AJ, Stone AJ, Fazeli F. Distributed Multipoles from a Robust Basis-Space Implementation of the Iterated Stockholder Atoms Procedure. J. Chem. Theory Comput. 2014; 10:5405–5418.

(87). Verstraelen T, Ayers PW, Van Speybroeck V, Waroquier M. The Conformational Sensitivity of Iterative Stockholder Partitioning Schemes. Chem. Phys. Lett. 2012; 545:138–143.

(88). Manz TA, Sholl DS. Chemically Meaningful Atomic Charges That Reproduce the Electrostatic Potential in Periodic and Nonperiodic Materials. J. Chem. Theory Comput. 2010; 6:2455–2468.

(89). Manz TA, Sholl DS. Improved Atoms-in-Molecule Charge Partitioning Functional for Simultaneously Reproducing the Electrostatic Potential and Chemical States in Periodic and Nonperiodic Materials. J. Chem. Theory Comput. 2012; 8:2844–2867.

(90). Lee LP, Limas NG, Cole DJ, Payne MC, Skylaris C-K, Manz TA. Expanding the Scope of Density Derived Electrostatic and Chemical Charge Partitioning to Thousands of Atoms. J. Chem. Theory Comput. 2014; 10:5377–5390.

(91). Verstraelen T, Sukhomlinov SV, Van Speybroeck V, Waroquier M, Smirnov KS. Computation of Charge Distribution and Electrostatic Potential in Silicates with the Use of Chemical Potential Equalization Models. J. Phys. Chem. C. 2012; 116:490–504.

(92). Kaduk B, Kowalczyk T, Van Voorhis T. Constrained Density Functional Theory. Chem. Rev. 2011; 112:321–370. [PubMed: 22077560]

(93). Momany FA. Determination of Partial Atomic Charges from ab initio Molecular Electrostatic Potentials. Application to Formamide, Methanol, and Formic Acid. J. Phys. Chem. 1978; 82:592–601.

(94). Cox SR, Williams DE. Representation of the Molecular Electrostatic Potential by a Net Atomic Charge Model. J. Comput. Chem. 1981; 2:304–323.

(95). Singh UC, Kollman PA. An Approach to Computing Electrostatic Charges for Molecules. J. Comput. Chem. 1984; 5:129–145.

(96). Besler BH, Merz KM, Kollman PA. Atomic Charges Derived from Semiempirical Methods. J. Comput. Chem. 1990; 11:431–439.

(97). Chirlian LE, Francl MM. Atomic Charges Derived from Electrostatic Potentials: A Detailed Study. J. Comput. Chem. 1987; 8:894–905.

(98). Breneman CM, Wiberg KB. Determining Atom-Centered Monopoles from Molecular Electrostatic Potentials. The Need for High Sampling Density in Formamide Conformational Analysis. J. Comput. Chem. 1990; 11:361–373.

(99). Stouch TR, Williams DE. Conformational Dependence of Electrostatic Potential Derived Charges of a Lipid Headgroup: Glycerylphosphorylcholine. J. Comput. Chem. 1992; 13:622–632.

(100). Stouch TR, Williams DE. Conformational Dependence of Electrostatic Potential-Derived Charges: Studies of the Fitting Procedure. J. Comput. Chem. 1993; 14:858–866.

(101). Bayly CI, Cieplak P, Cornell W, Kollman PA. A Well-Behaved Electrostatic Potential Based Method Using Charge Restraints for Deriving Atomic Charges: the RESP Model. J. Phys. Chem. 1993; 97:10269–10280.

(102). Berente I, Czinki E, Naray-szabo G. A Combined Electronegativity Equalization and Electrostatic Potential Fit Method for the Determination of Atomic Point Charges. J. Comput. Chem. 2007; 28:1936–1942. [PubMed: 17450564]

(103). Hu H, Lu Z, Yang W. Fitting Molecular Electrostatic Potentials from Quantum Mechanical Calculations. J. Chem. Theory Comput. 2007; 3:1004–1013.

(104). Zeng J, Duan L, Zhang JZH, Mei Y. A Numerically Stable Restrained Electrostatic Potential Charge Fitting Method. J. Comput. Chem. 2013; 34:847–853. [PubMed: 23281029]

(105). Morita A, Kato S. Molecular Dynamics Simulation with the Charge Response Kernel: Diffusion Dynamics of Pyrazine and Pyrazinyl Radical in Methanol. J. Chem. Phys. 1998; 108:6809–6818.

(106). Herbert JM, Jacobson LD, Lao KU, Rohrdanz MA. Rapid Computation of Intermolecular Interactions in Molecular and Ionic Clusters: Self-Consistent Polarization Plus Symmetry-Adapted Perturbation Theory. Phys. Chem. Chem. Phys. 2012; 14:7679–7699. [PubMed: 22511183]

(107). Holden ZC, Richard RM, Herbert JM. Periodic Boundary Conditions for QM/MM Calculations: Ewald Summation for Extended Gaussian Basis Sets. J. Chem. Phys. 2013; 139:244108. [PubMed: 24387358]

(108). Li J, Zhu T, Cramer CJ, Truhlar DG. New Class IV Charge Model for Extracting Accurate Partial Charges from Wave Functions. J. Phys. Chem. A. 1998; 102:1820–1831.

(109). Li J, Williams B, Cramer CJ, Truhlar DG. A Class IV Charge Model for Molecular Excited States. J. Chem. Phys. 1999; 110:724–733.

(110). Winget P, Thompson JD, Xidos JD, Cramer CJ, Truhlar DG. Charge Model 3: A Class IV Charge Model Based on Hybrid Density Functional Theory with Variable Exchange. J. Phys. Chem. A. 2002; 106:10707–10717.

(111). Vilseck JZ, Tirado-Rives J, Jorgensen WL. Evaluation of CM5 Charges for Condensed-Phase Modeling. J. Chem. Theory Comput. 2014; 10:2802–2812. [PubMed: 25061445]

(112). Medders GR, Paesani F. Many-Body Convergence of the Electrostatic Properties of Water. J. Chem. Theory Comput. 2013; 9:4844–4852.

(113). Shao Y, Gan Z, Epifanovsky E, Gilbert AT, Wormit M, Kussmann J, Lange AW, Behn A, Deng J, Feng X, et al. Advances in Molecular Quantum Chemistry Contained in the Q-Chem 4 Program Package. Mol. Phys. 2015; 113:184–215.

(114). Jurecka P, Sponer J, Cerny J, Hobza P. Benchmark Database of Accurate (MP2 and CCSD(T) Complete Basis Set Limit) Interaction Energies of Small Model Complexes, DNA Base Pairs, and Amino Acid Pairs. Phys. Chem. Chem. Phys. 2006; 8:1985–1993. [PubMed: 16633685]

(115). Lee C, Yang W, Parr RG. Development of the Colle-Salvetti Correlation-Energy Formula into a Functional of the Electron Density. Phys. Rev. B. 1988; 37:785–789.

(116). Zhao Y, Truhlar DG. The M06 Suite of Density Functionals for Main Group Thermochemistry, Thermochemical Kinetics, Noncovalent Interactions, Excited States, and Transition Elements: Two New Functionals and Systematic Testing of Four M06-Class Functionals and 12 Other Functionals. Theor. Chem. Acc. 2008; 120:215–241.

(117). Chai J-D, Head-Gordon M. Long-Range Corrected Hybrid Density Functionals with Damped Atom-Atom Dispersion Corrections. Phys. Chem. Chem. Phys. 2008; 10:6615–6620. [PubMed: 18989472]

(118). Elking DM, Perera L, Pedersen LG. HPAM: Hirshfeld partitioned atomic multipoles. Comput. Phys. Commun. 2012; 183:390–397. [PubMed: 22140274]

(119). Truchon J-F, Nicholls A, Iftimie RI, Roux B, Bayly CI. Accurate Molecular Polarizabilities Based on Continuum Electrostatics. J. Chem. Theory Comput. 2008; 4:1480–1493. [PubMed: 23646034]

(120). Kramer C, Gedeck P, Meuwly M. Atomic Multipoles: Electrostatic Potential Fit, Local Reference Axis Systems, and Conformational Dependence. J. Comput. Chem. 2012; 33:1673–1688. [PubMed: 22544510]

(121). Ghosh D, Kosenkov D, Vanovschi V, Williams CF, Herbert JM, Gordon MS, Schmidt MW, Slipchenko LV, Krylov AI. Noncovalent Interactions in Extended Systems Described by the Effective Fragment Potential Method: Theory and Application to Nucleobase Oligomers. J. Phys. Chem. A. 2010; 114:12739–12754. [PubMed: 21067134]

(122). in het Panhuis M, Popelier PLA, Munn RW, Angyan JG. Distributed Polarizability of the Water Dimer: Field-Induced Charge Transfer Along the Hydrogen Bond. J. Chem. Phys. 2001; 114:7951–7961.

(123). Tkatchenko A, DiStasio RA, Car R, Scheffler M. Accurate and Efficient Method for Many-Body van der Waals Interactions. Phys. Rev. Lett. 2012; 108:236402. [PubMed: 23003978]

(124). DiStasio RA Jr. Gobre VV, Tkatchenko A. Many-Body van der Waals Interactions in Molecules and Condensed Matter. J. Phys.: Condens. Mat. 2014; 26:213202.

(125). Kuhs, WF.; Lehmann, MS. In Water Science Reviews 2. Franks, F., editor. Vol. Vol. 2. Cambridge University Press; 1986. p. 1-66.Cambridge Books Online

(126). Marenich AV, Cramer CJ, Truhlar DG. Reduced and Quenched Polarizabilities of Interior Atoms in Molecules. Chem. Sci. 2013; 4:2349–2356.

(127). Gordon MS, Smith QA, Xu P, Slipchenko LV. Accurate First Principles Model Potentials for Intermolecular Interactions. Annu. Rev. Phys. Chem. 2013; 64:553–578. [PubMed: 23561011]

(128). Yu H, Hansson T, van Gunsteren WF. Development of a Simple, Self-Consistent Polarizable Model for Liquid Water. J. Chem. Phys. 2003; 118:221–234.

(129). Lamoureux G, MacKerell AD, Roux B. A Simple Polarizable Model of Water Based on Classical Drude Oscillators. J. Chem. Phys. 2003; 119:5185–5197.

(130). Geerke DP, van Gunsteren WF. The Performance of Non-Polarizable and Polarizable Force-Field Parameter Sets for Ethylene Glycol in Molecular Dynamics Simulations of the Pure Liquid and Its Aqueous Mixtures. Mol. Phys. 2007; 105:1861–1881.

(131). Anisimov VM, Vorobyov IV, Roux B, MacKerell AD. Polarizable Empirical Force Field for the Primary and Secondary Alcohol Series Based on the Classical Drude Model. J. Chem. Theory Comput. 2007; 3:1927–1946. [PubMed: 18802495]

(132). Schropp B, Tavan P. The Polarizability of Point-Polarizable Water Models: Density Functional Theory/Molecular Mechanics Results. J. Phys. Chem. B. 2008; 112:6233–6240. [PubMed: 18198859]

(133). Vosmeer CR, Rustenburg AS, Rice JE, Horn HW, Swope WC, Geerke DP. QM/MM-Based Fitting of Atomic Polarizabilities for Use in Condensed-Phase Biomolecular Simulation. J. Chem. Theory Comput. 2012; 8:3839–3853.

(134). Khaliullin RZ, Bell AT, Head-Gordon M. Electron Donation in the Water-Water Hydrogen Bond. Chem. Eur. J. 2009; 15:851–855. [PubMed: 19086050]

(135). Wu Q, Ayers PW, Zhang Y. Density-Based Energy Decomposition Analysis for Intermolecular Interactions with Variationally Determined Intermediate State Energies. J. Chem. Phys. 2009; 131:164112. [PubMed: 19894932]

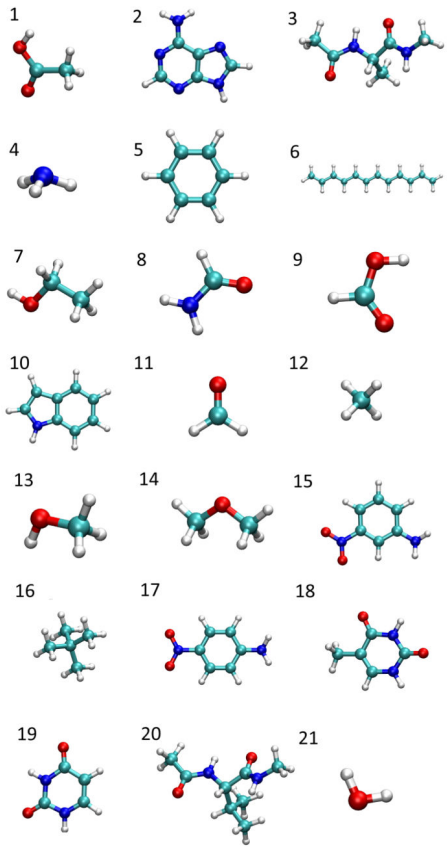

Fig. 1.

Monomers studied in this work. 1. Acetic acid. 2. Adenine. 3. Alanine dipeptide. 4. Ammonia. 5. Benzene. 6. Dodecahexene. 7. Ethanol. 8. Formamide. 9. Formic acid. 10. Indole. 11. Methanal. 12. Methane. 13. Methanol. 14. Methyl ether. 15. m-Nitroaniline (mNA). 16. Neopentane. 17. p-Nitroaniline (pNA). 18. Thymine. 19. Uracil. 20. Valine dipeptide. 21. Water.

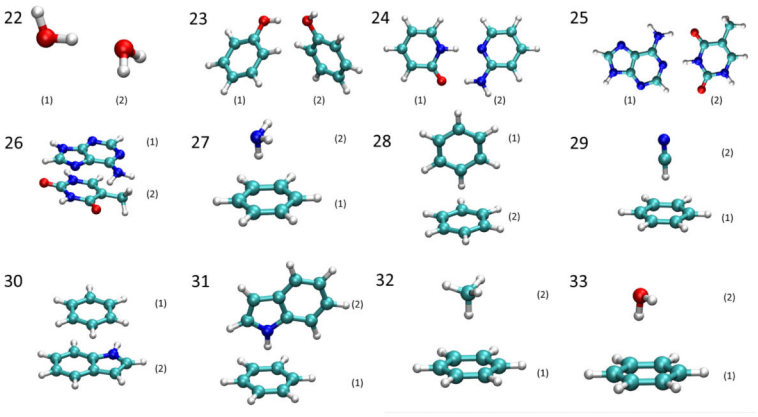

Fig. 2.

Dimers chosen from the S22 database. 22. water dimer. 23. phenol dimer. 24. 2-pyridoxine/2-aminopyridine complex. 25. Hydrogen-bonded adenine/thymine complex. 26. Stacked adenine/thymine complex. 27. Benzene/ammonia complex. 28. T-shaped benzene dimer. 29. Benzene/HCN complex. 30. Stacked benzene/indole. 31. T-shaped benzene/indole complex. 32. Benzene/methane complex. 33. Benzene/water complex. Numbers in the parentheses are the sequences of the monomers in each dimer.

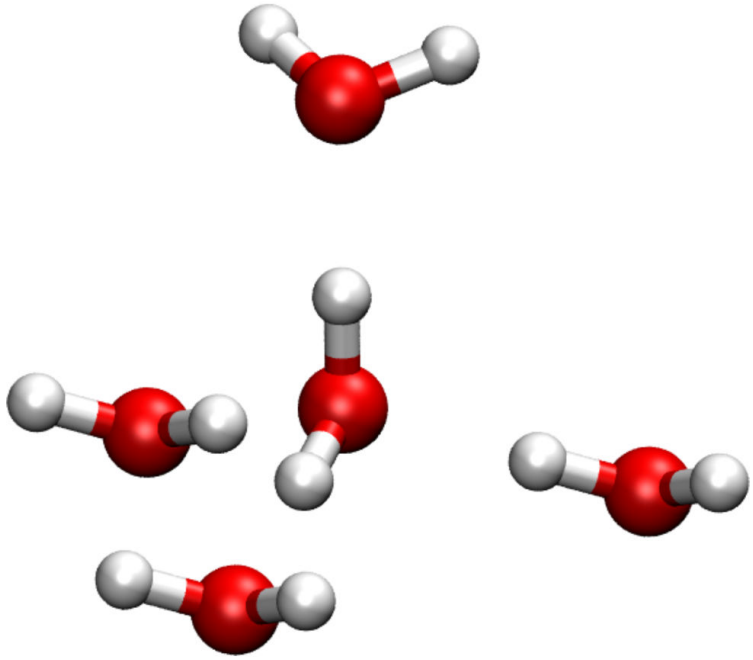

Fig. 3.

A water pentamer extracted from ice Ih,[125] in which the central water molecule interacts with the other four water molecules through hydrogen bonds.

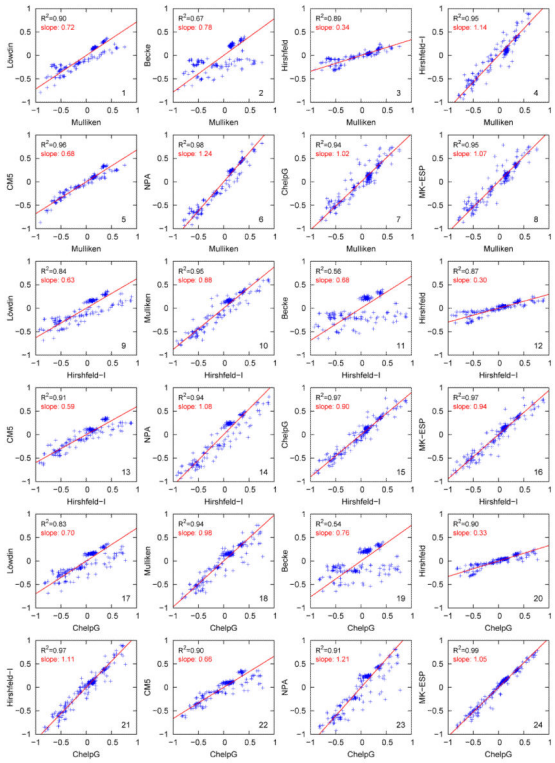

Fig. 4.

Correlation among various charge definitions for the monomers calculated at the B3LYP/6-31G(d) level of theory.

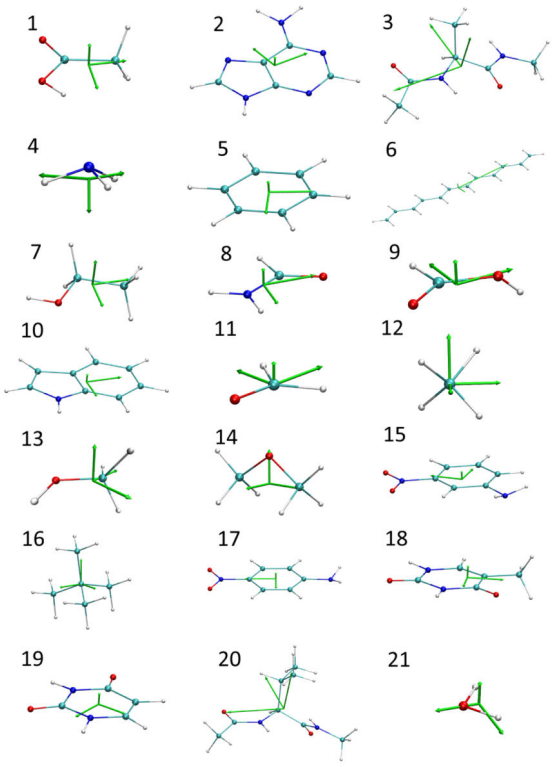

Fig. 5.

Molecular polarizability tensor shown as green arrows. The atoms and covalent bonds have been shrunk to make the tensors presented more clearly.

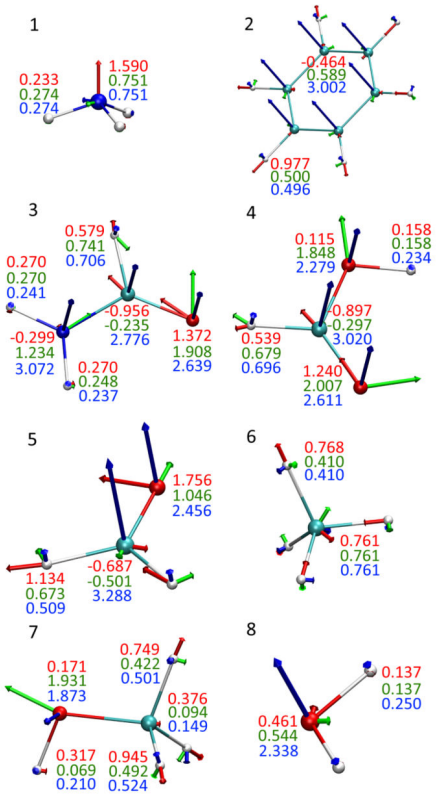

Fig. 6.

Atomic polarizability $\left(\hat{\boldsymbol{\alpha}}^{IAD}\right)$ under Hirshfeld-I scheme for 1. Ammonia. 2. Benzene. 3. Formamide. 4. Formic acid. 5. Methanal. 6. Methane. 7. Methanol. 8. Water.

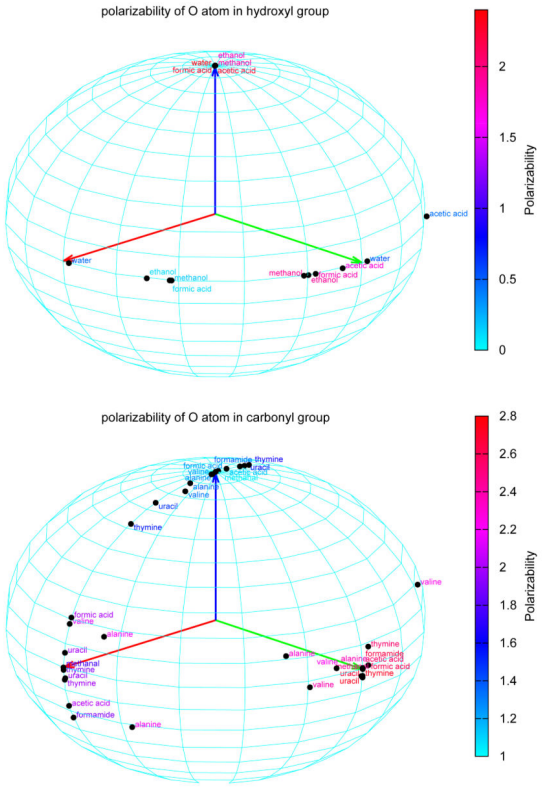

Fig. 7.
Atomic polarizabilities from various functional groups.

Table 1

Atomic charge fluctuation (a.u.) among different basis sets and density functionals measured by Eq. 20.

charge definition	Löwdin	Mulliken	Becke	Hirshfeld (CM5)	Hirshfeld-I	NPA	CHELPG	MK-ESP
χ_{basis}	0.1617	0.1790	0.0031	0.0039	0.0295	0.0234	0.0253	0.0302
$\chi_{functional}$	0.0016	0.0050	0.0014	0.0014	0.0067	0.0019	0.0039	0.0039

Table 2

QM molecular dipole moments (in debye) from B3LYP/6-31G(d) calculations and those computed from atomic charges within various charge models (first term in Eq. 13). Molecules with zero dipole moments (benzene, dodecahexene, methane and neopentane) are excluded. Relative differences in the dipole moments are shown in parentheses, with the mean relative difference (MRD) listed in the last row.

	QM	Löwdin	Mulliken	Becke	Hirshfeld	Hirshfeld-I	CM5	NPA	CHELPG	MK-ESP
acetic acid	4.40	4.09	5.01	4.08	2.87	4.38	4.22	6.02	4.43	4.41
		(−7.0%)	(13.9%)	(−7.3%)	(−34.8%)	(−0.5%)	(−4.1%)	(36.8%)	(0.7%)	(0.2%)
adenine	2.66	2.11	2.38	2.24	1.84	2.67	2.42	2.85	2.69	2.71
		(−20.7%)	(−10.5%)	(−15.8%)	(−30.8%)	(0.4%)	(−9.0%)	(7.1%)	(1.1%)	(1.9%)
alanine	3.11	3.31	2.87	3.46	2.81	3.04	3.02	3.60	3.11	3.13
		(6.4%)	(−7.7%)	(11.3%)	(−9.6%)	(−2.3%)	(−2.9%)	(15.8%)	(0.0%)	(0.6%)
ammonia	1.70	1.26	1.45	1.17	0.48	1.80	1.39	1.78	1.75	1.77
		(−25.9%)	(−14.7%)	(−31.2%)	(−71.8%)	(5.9%)	(−18.2%)	(4.7%)	(2.9%)	(4.1%)
ethanol	1.56	1.67	2.14	1.17	0.70	1.73	1.48	2.99	1.56	1.56
		(7.1%)	(37.2%)	(−25.0%)	(−55.1%)	(10.9%)	(−5.1%)	(91.7%)	(0.0%)	(0.0%)
formamide	3.82	3.47	3.83	3.44	2.84	3.69	3.53	4.94	3.83	3.82
		(−9.2%)	(0.3%)	(−9.9%)	(−25.7%)	(−3.4%)	(−7.6%)	(29.3%)	(0.3%)	(0.0%)
formic acid	1.75	1.57	1.54	2.00	1.62	1.70	1.68	1.88	1.76	1.76
		(−10.3%)	(−12.0%)	(14.3%)	(−7.4%)	(−2.9%)	(−4.0%)	(7.4%)	(0.6%)	(0.6%)
indole	2.19	2.04	0.98	2.30	1.89	2.27	1.85	1.78	2.18	2.19
		(−6.8%)	(−55.3%)	(5.0%)	(−13.7%)	(3.7%)	(−15.5%)	(−18.7%)	(−0.5%)	(0.0%)
methanal	2.19	1.82	2.56	1.47	1.42	2.05	2.10	3.63	2.22	2.21
		(−16.9%)	(16.9%)	(−32.9%)	(−35.2%)	(−6.4%)	(−4.1%)	(65.8%)	(1.4%)	(0.9%)
methanol	1.69	1.79	2.27	1.46	0.77	1.69	1.59	2.96	1.70	1.70
		(5.9%)	(34.3%)	(−13.6%)	(−54.4%)	(0.0%)	(−5.9%)	(75.1%)	(0.6%)	(0.6%)
methyl ether	1.27	1.60	2.21	1.33	0.64	0.91	1.38	2.99	1.33	1.32
		(26.0%)	(74.0%)	(4.7%)	(−49.6%)	(−28.3%)	(8.7%)	(135.4%)	(4.7%)	(3.9%)
mNA	5.65	5.67	7.10	6.07	4.59	5.37	5.39	6.94	5.74	5.72
		(0.4%)	(25.7%)	(7.4%)	(−18.8%)	(−5.0%)	(−4.6%)	(22.8%)	(1.6%)	(1.2%)
pNA	7.12	7.17	8.22	7.65	6.00	6.80	6.83	8.32	7.19	7.18
		(0.7%)	(15.4%)	(7.4%)	(−15.7%)	(−4.5%)	(−4.1%)	(16.9%)	(1.0%)	(0.8%)

	QM	Löwdin	Mulliken	Becke	Hirshfeld	Hirshfeld-I	CM5	NPA	CHELPG	MK-ESP
thymine	4.29	3.89	5.00	3.65	3.39	4.11	4.01	5.96	4.29	4.26
		(−9.3%)	(16.6%)	(−14.9%)	(−21.0%)	(−4.2%)	(−6.5%)	(38.9%)	(0.0%)	(−0.7%)
uracil	4.32	3.89	5.07	3.47	3.45	4.31	4.03	5.95	4.37	4.36
		(−10.0%)	(17.4%)	(−19.7%)	(−20.1%)	(−0.2%)	(−6.7%)	(37.7%)	(1.2%)	(0.9%)
valine	2.88	3.15	2.69	3.51	2.71	2.79	2.80	3.19	2.91	2.90
		(9.4%)	(−6.6%)	(21.9%)	(−5.9%)	(−3.1%)	(−2.8%)	(10.8%)	(1.0%)	(0.7%)
water	2.08	1.94	2.20	1.82	0.89	2.41	1.83	2.64	2.14	2.14
		(−6.7%)	(5.8%)	(−12.5%)	(−57.2%)	(15.9%)	(−12.0%)	(26.9%)	(2.9%)	(2.9%)
RMSD[1]		0.36	0.87	0.66	0.94	0.25	0.24	1.24	0.06	0.06
RMSD[2]		0.30	0.69	0.47	0.90	0.18	0.22	1.14	0.04	0.04
MRD		(−3.9%)	(8.9%)	(−6.5%)	(−31.0%)	(−1.4%)	(−6.2%)	(35.6%)	(1.1%)	(1.1%)

J Phys Chem A. Author manuscript; available in PMC 2015 July 31.

Table 3

Angles (in degree) between the QM dipole and the dipoles computed from atomic charges.

	Löwdin	Mulliken	Becke	Hirshfeld	Hirshfeld-I	CM5	NPA	CHELPG	MK-ESP
acetic acid	2.74	7.49	2.29	2.74	2.48	0.35	4.62	0.29	0.16
adenine	12.06	10.23	20.96	18.58	5.28	4.98	7.77	1.81	2.30
alanine	1.50	2.33	9.29	2.40	5.22	2.03	1.89	1.14	0.75
ammonia	0.32	0.00	0.00	0.00	0.00	0.00	0.00	0.01	0.14
ethanol	11.96	17.19	6.13	9.27	8.22	2.68	20.75	1.49	1.08
formamide	1.53	7.47	6.32	1.37	2.89	2.05	10.31	0.38	0.55
formic acid	7.19	13.69	19.24	7.30	2.16	1.13	25.06	1.15	1.09
indole	2.44	17.49	6.30	3.80	0.94	3.44	3.58	0.08	0.03
methanal	0.00	0.00	0.00	0.00	0.00	0.00	0.00	0.05	0.00
methanol	9.22	16.00	10.94	5.05	6.28	1.26	19.06	1.33	1.04
methyl ether	0.00	0.00	0.00	0.00	0.00	0.00	0.00	0.08	0.00
mNA	2.12	9.10	4.94	6.71	2.08	0.32	6.78	0.82	0.98
pNA	1.36	0.85	1.56	4.28	1.41	0.18	0.24	0.64	0.74
thymine	1.67	12.35	4.78	1.60	1.79	2.13	4.11	0.69	0.33
uracil	2.56	10.94	9.15	2.32	2.76	1.20	6.63	0.40	0.27
valine	1.54	3.22	18.98	6.30	7.19	2.44	4.23	0.67	0.19
water	0.10	0.08	0.48	0.40	0.03	0.03	0.22	0.02	0.12
Average	3.43	7.55	7.14	4.24	2.87	1.42	6.78	0.65	0.57

Table 4

Slope and R^2 values (in parentheses) for the correlation among atomic charges from different charge schemes.

		Löwdin	Mulliken	Becke	Hirshfeld	Hirshfeld-I	CM5	NPA	CHELPG	MK-ESP
Löwdin	slope		0.72	0.92	2.12	0.63	1.06	0.58	0.70	0.67
	R^2		(0.90)	(0.91)	(0.84)	(0.84)	(0.91)	(0.95)	(0.83)	(0.86)
Mulliken	slope	1.40		1.28	2.97	0.88	1.48	0.81	0.98	0.93
	R^2	(0.90)		(0.67)	(0.89)	(0.95)	(0.96)	(0.98)	(0.94)	(0.95)
Becke	slope	1.09	0.78		2.31	0.68	1.15	0.63	0.76	0.73
	R^2	(0.91)	(0.67)		(0.60)	(0.56)	(0.72)	(0.75)	(0.54)	(0.60)
Hirshfeld	slope	0.47	0.34	0.43		0.30	0.50	0.27	0.33	0.31
	R^2	(0.84)	(0.89)	(0.60)		(0.87)	(0.89)	(0.89)	(0.90)	(0.80)
Hirshfeld-I	slope	1.59	1.14	1.46	3.38		1.68	0.92	1.11	1.06
	R^2	(0.84)	(0.95)	(0.56)	(0.87)		(0.91)	(0.94)	(0.94)	(0.97)
CM5	slope	0.95	0.68	0.87	2.01	0.59		0.55	0.66	0.63
	R^2	(0.91)	(0.96)	(0.72)	(0.89)	(0.91)		(0.95)	(0.90)	(0.90)
NPA	slope	1.73	1.24	1.59	3.67	1.08	1.82		1.21	1.15
	R^2	(0.95)	(0.98)	(0.75)	(0.89)	(0.94)	(0.95)		(0.91)	(0.94)
CHELPG	slope	1.43	1.02	1.31	3.04	0.90	1.51	0.83		0.95
	R^2	(0.83)	(0.94)	(0.54)	(0.90)	(0.97)	(0.90)	(0.91)		(0.99)
MK-ESP	slope	1.50	1.07	1.38	3.18	0.94	1.58	0.87	1.05	
	R^2	(0.86)	(0.95)	(0.60)	(0.88)	(0.97)	(0.90)	(0.94)	(0.99)	

Table 5

Root-mean-square-fluctuations (RMSF) of the amount of charge transfer between monomers calculated at the B3LYP level of theory with 9 basis sets

charge definition	Löwdin	Mulliken	Becke	Hirshfeld	Hirshfeld-I	CM5	NPA	CHELPG	MK-ESP
RMSF	0.0187	0.0418	0.0023	0.0041	0.0062	0.0041	0.0023	0.0050	0.0069

Table 6

Charge transfer from the 2nd molecule to the 1st molecule at the B3LYP/6-31G(d) level of theory for the dimers in Fig. 2 (units: a.u.). For each molecule (and the averages), the underlined values correspond to the smallest amount of charge transfer, while the bold-faced values highlight the largest amount of charge transfer.

	Löwdin	Mulliken	Becke	Hirshfeld	Hirshfeld-I	CM5	NPA	CHELPG	MK-ESP
water dimer	−0.055	−0.053	0.005	**−0.100**	−0.054	−0.086	−0.027	−0.038	−0.040
phenol dimer	−0.047	−0.040	0.020	**−0.097**	−0.057	−0.081	−0.023	−0.027	−0.041
2-pyridoxine/2-aminopyridine	−0.031	−0.022	−0.025	−0.038	−0.033	−0.032	−0.016	−0.086	**−0.144**
Adenine/Thymine H-bonded	0.035	0.021	0.047	0.041	0.026	0.032	0.026	0.054	**0.078**
Adenine/Thymine stacked	0.016	0.015	−0.018	0.030	0.022	0.024	0.012	0.043	**0.048**
benzene/ammonia	0.007	0.013	**−0.054**	0.043	0.029	0.041	0.003	0.016	0.025
benzene/benzene T-Shaped	−0.009	−0.017	**0.053**	−0.048	−0.040	−0.043	−0.005	−0.017	−0.041
benzene/HCN	0.021	0.032	−0.033	0.072	0.057	0.067	0.010	0.058	**0.084**
benzene/indole stacked	−0.011	−0.012	**0.025**	−0.021	−0.020	−0.018	−0.009	−0.011	−0.011
benzene/indole T-Shaped	0.021	0.034	−0.037	**0.089**	0.066	0.085	0.009	0.046	0.076
benzene/methane	0.004	0.010	**−0.068**	0.032	0.026	0.029	0.003	0.006	0.013
benzene/water	0.014	0.021	−0.041	**0.061**	0.037	0.058	0.005	0.038	0.046
mean signed average	−0.003	0.000	−0.011	0.005	0.005	0.006	−0.001	0.007	0.008
mean unsigned average	0.023	0.024	0.036	**0.056**	0.039	0.050	0.012	0.037	0.054

Table 7

Molecular polarizability (a.u.) and anisotropy computed at the B3LYP/6-31G(d) level of theory.

	polarizability			anisotropy		polarizability			anisotropy
acetic acid	18.29	28.18	33.57	0.503	adenine	31.02	92.38	108.07	0.914
alanine	107.20	78.59	59.83	0.505	ammonia	5.12	9.10	9.10	0.511
benzene	20.99	75.11	75.11	0.948	dodecahexene	552.60	105.61	42.69	2.061
ethanol	29.70	25.72	23.80	0.198	formamide	28.46	21.70	9.67	0.826
formic acid	19.21	21.12	8.84	0.698	indole	125.88	95.55	29.54	1.020
methanal	14.13	18.35	6.76	0.777	methane	12.36	12.36	12.36	0.000
methanol	17.71	15.41	14.00	0.207	methyl ether	30.96	24.49	24.17	0.250
mNA	115.13	98.80	29.64	0.968	neopentane	53.44	53.43	53.44	0.000
pNA	138.87	29.45	95.64	1.085	thymine	94.29	72.01	32.72	0.814
uracil	23.68	61.98	79.26	0.896	valine	120.57	98.17	87.43	0.287
water	7.25	5.31	2.84	0.746					

Table 8

The percentage of charge fluctuation contributions to the total molecular polarizability of 21 molecules, as defined in Eq. 22 using different charge schemes.

	Löwdin	Mulliken	Becke	Hirshfeld (CM5)	Hirshfeld-I	NPA	CHELPG	MK-ESP
acetic acid	62.41	93.27	59.33	56.90	74.84	63.97	93.99	94.52
adenine	72.20	90.30	70.28	69.59	80.90	71.38	91.33	92.08
alanine	70.48	106.17	67.69	66.45	80.94	68.36	98.68	99.19
ammonia	47.11	83.87	44.13	39.16	76.69	55.01	94.84	95.73
benzene	73.32	104.17	69.36	68.07	82.13	73.92	86.53	87.29
dodecahexene	86.66	101.49	84.80	84.17	91.35	86.64	93.24	93.65
ethanol	62.86	109.12	58.34	55.73	79.20	65.67	97.46	98.53
formamide	61.16	85.11	57.26	55.08	74.80	64.48	82.03	82.78
formic acid	56.63	76.11	52.88	50.94	70.74	59.51	80.30	80.83
indole	75.68	102.60	72.67	71.83	83.45	75.10	87.24	87.83
methanal	53.50	82.21	49.92	46.43	69.44	60.48	79.57	80.75
methane	59.29	115.66	51.67	45.48	76.70	66.27	94.97	96.48
methanol	58.40	99.43	53.70	50.29	77.11	63.43	95.91	97.12
methyl ether	62.88	106.10	58.67	55.46	78.78	65.41	96.99	98.06
mNA	74.62	94.78	72.54	71.69	82.54	74.29	91.85	92.53
neopentane	67.84	121.09	64.04	61.52	81.84	66.77	97.69	98.82
pNA	76.80	95.08	74.75	73.86	84.24	76.77	91.98	92.61
thymine	71.93	95.14	69.64	68.26	80.34	71.28	93.51	94.27
uracil	71.02	89.43	68.76	67.35	79.11	71.05	88.44	90.68
valine	70.77	109.47	68.32	67.03	81.92	68.18	98.78	99.32
water	38.52	60.61	37.03	33.52	71.45	47.32	78.74	79.14
average	65.43	96.25	62.18	59.94	78.98	67.40	91.15	92.01

Table 9

The principal polarizability components (a.u.) of the oxygen atoms in the water pentamer and the net charge of each water molecule under Hirshfeld and Hirshfeld-I schemes. x: the direction perpendicular to the water plane. y: the direction bifurcating the hydrogen atoms. z: the direction perpendicular to the x-y plane.

	Hirshfeld					Hirshfeld-I				
	polarizability				net charge	polarizability				net charge
	x	y	z	average		x	y	z	average	
central	1.63	1.61	1.61	1.61	0.004	2.46	1.50	1.08	1.68	0.005
acceptor	1.90	1.94	1.86	1.90	0.139	2.50	0.76	0.30	1.19	0.076
donor	1.96	2.23	2.04	2.08	−0.141	2.27	1.39	0.42	1.36	−0.078